Thesis

Imperial College London

Materials - MPhil (2020)

Materials and morphogen gradients-guided brain organoid anteroposterior polarization study

Juzhi Zhao

CID: [redacted]

Supervised by Professor Molly M. Stevens

Materials and Bioengineering and the Institute of Biomedical Engineering

Abstract:

Brain organoids deriving from human pluripotent stem cells are highly advanced *in vitro* models recapitulating many features of the developing brain. However, the lack of predictable anatomy and spatial organization has restricted the breadth of applications for which brain organoids can be used. In nature, the human brain develops from an elongated structure known as the neural tube, which further polarized via the coordinated action of multiple morphogens (e. g. Wnt, SHH, BMP) that spatially regulate cell fate specification in a concentration-dependent manner. Microfluidic platforms with high controllability on microflows are known to be useful for generating concentration gradients with sequential mixing microchannels. Biocompatible materials were proven to be effective in regulating the shape of brain organoids. In this study, a novel platform with an in-house microfluidic gradient generator and material-guided elongated brain organoid was established, providing a new methodology for brain organoid anteroposterior patterning studies. To optimize and develop the patterning protocol, the influence of dual SMADi and SAG on brain organoid growth with different exposure periods was investigated. Materials including silk fiber, PCL, and PDO suture threads were tested for elongated brain organoid generation, revealing the effect of material properties and sizes on guiding organoid growth. Future analysis and deeper illustration of complex gene expression and signaling pathways included in the neural tube anteroposterior patterning process can also be performed based on this study.

Declaration of Originality

I, Juzhi Zhao, declare that this is my original scientific work content reported within this thesis, and was acquired and analyzed by myself at Imperial College London, unless otherwise stated. All collaborative efforts are noted by name.

Copyright declaration

The copyright of this thesis rests with the author. Unless otherwise indicated, its contents are licensed under a Creative Commons Attribution-Non Commercial 4.0 International Licence (CC BY-NC).

Under this licence, you may copy and redistribute the material in any medium or format. You may also create and distribute modified versions of the work. This is on the condition that: you credit the author and do not use it, or any derivative works, for a commercial purpose.

When reusing or sharing this work, ensure you make the licence terms clear to others by naming the licence and linking to the licence text. Where a work has been adapted, you should indicate that the work has been changed and describe those changes.

Please seek permission from the copyright holder for uses of this work that are not included in this licence or permitted under UK Copyright Law.

Acknowledgement

I would like to thank Professor Molly Stevens for welcoming me to this magnificent group. From her, I learned the inclusiveness and farsightedness of a great scientist. I have been fascinated by how multi-disciplinary and advanced the Stevens Group has been. With approximately 100 scientists working together as a family, not only bring out a considerable number of possibilities to cooperate, but also greatly promote scientific imagination and vitality. I conducted this MPhil project and another MRes project in this group. My supervisors, Dr. Daniel Hachim and Dr. Ruoxiao Xie, have given me the kindest support and instructions. No matter in or outside the lab, they are my wonderful teachers and close friends. Thanks to Dr. Kaja Ritzau-Reid, who introduced me to the field of brain organoid and taught me every skill I needed to know. Thanks to Dr. Richard Wang for his great help in building up the microfluidic gradient generator and the guidance in the field of engineering. Their rigorous research style has shown me the demeanor and charm of conducting laboratory work.

Meanwhile, I especially appreciated the help from Dr. James Armstrong, who edited my every article and attended every update meeting even after he left the group. His wise and profound insight into life science has undoubtedly made me a better scientist. I also enjoyed the time I spent with my beloved friends and my 2020 cohort in the group. Thanks for the sharing and chatting from Xin, Shiyang, Francesca, Camille, Lino, Schan, Aida, Gwen, and Lukeria. Last but not least, thanks to our data manager Akemi for making it so much easier. Thanks to Brittany, Lucy, Dennis, and all the support group members for making this project possible.

I have spent three years in this group and in this beautiful country. Life experience here is invaluable, showered me with British culture, built up my character, and inspired me a lot about my future path. My parents supported me both financially and emotionally during this beautiful journey. I will look back with gratitude and work passionately with all the lessons I have learned.

Contents index

List of abbreviations 7
List of tables 9
List of figures 9
1. Background introduction 11
1.1 Cerebral Organoid 11
1.2 Applications of cerebral organoids 13
1.3 Limitations of brain organoids 14
1.4 Assembloids 15
1.5 Brain regionalization and brain organoid polarization 17
1.6 Microfluidic gradient generator 19
1.7 Scaffold mediated brain organoid 22
2 Hypothesis, aims and objectives 25
3 Material and methods 26
3.1 Microfluidic gradient generator 26
3.1.1 The microfluidic chip and cell crown design 26
3.1.2 PDMS microfluidic chip and cell crown fabrication 26
3.1.3 Brain organoid culture within the microfluidic chip 27
3.1.4 Gradient visualization 28
3.2 Round cerebral organoid cultivation 28
3.2.1 Organoid culture media 28
3.2.2 H9 cell maintaining 29
3.2.3 Cerebral organoid cultivation 29
3.3 Brain organoid elongation 30
3.3.1 Material biocompatibility examination 30
3.3.2 Organoid elongation with 27G PDO 30
3.3.3 20G PDO/PCL-guided elongated organoid 31
3.4 Anteroposterior microfluidic patterning 31
3.5 Brain organoid characterization 33

3.5.1 Cryosection 33
3.5.2 Organoid sections immunostaining 33
3.5.3 Confocal microscopy imaging 34
3.5.4 RNA extraction 34
3.5.5 cDNA reverse transcription 34
3.5.6 qRT-PCR 35
3.6 data analysis 35
4 Results 36
4.1 Specific aims 36
4.2 Microfluidic concentration gradient generator 36
4.2.1 Microfluidic chip characterization and optimization 36
4.2.2 Microfluidic gradient visualization 38
4.3 Caudal and rostral protocol for microfluidic patterning 38
4.3.1 Short-term culture 38
4.3.2 Long-term culture 42
4.4 Material screening 44
4.4.1 Scaffold materials 44
4.4.2 Brain organoid viability test 45
4.5 Anteroposterior patterning with microfluidic platform 47
4.5.1 Elongated organoid preliminary experiments 47
4.5.2 Anteroposterior patterning with microfluidic platform 49
5 Discussion 51
5.1 Microfluidic based brain organoid polarization platform 51
5.2. Morphogen regulations for 20-day brain organoid anteroposterior patterning 52
5.3 Long-term culture 55
5.4 Elongated brain organoid generation 56
6. Future work 58
7. Conclusion 59
References 62
Supplementary materials 69

List of abbreviations

AA	L-Ascorbic Acid
AD	Alzheimer's disease
APOE	Apolipoprotein E gene
aPKCζ	Apical protein kinase C
Auto CAD	Autodesk Computer Aided Design
BDNF	Brain-derived neurotrophic factor
BF	Bright field
BMP	Bone morphogenic protein
BoC	Brain-on-a-chip
BSA	Bovine albumin
cAMP	Cyclic adenosine monophosphate
CDK5RAP2	CDK5 regulatory subunit-associated protein 2
CNS	Central nervous system
CHIR	CHIR99021
CP	Cortical plate
CRISPR	Clustered regularly interspaced short palindromic repeats
CTIP2	BAF Chromatin Remodeling Complex Subunit BCL11B
DAPI	4',6-diamidino-2-phenylindole
DCX	Doublecortex
DMEM	Dulbecco’s modified Eagle’s medium
DM	Dorsomorphin
Dual SMADi	Dual SMAD inhibition
EB	Embryo bodies
ECM	Extracellular matrix
EHS	Engelbreth-Holm-Swarm
EGF	Epidermal growth factor
enCORs	Engineered cerebral organoids
EP	Eppendorf
FGF	Fibroblast growth factor
FOXA2	Forkhead Box A2
FOXG1	Forkhead Box G1
FSS	Fluorescein sodium salt
GABA	Aminobutyric acid

GAPDH	Glyceraldehyde-3-phosphate dehydrogenase
GBX2	Gastrulation and brain-specific homeobox protein 2
GFP	Green fluorescent protein
GSK3i	Glycogen synthase kinase 3 inhibitor
H&E	Hematoxylin and Eosin kit
hESC	Human embryo stem cell
HOX	Homeotic genes
IGF-1	Insulin-like growth factors -1
IPA	Isopropanol absolute
iPSC	Induced pluripotent stem cells
MAP2	Microtubule Associated Protein 2
MG	Matrigel
MHB	Midbrain-hindbrain boundary
NG	Noggin
OLIG2	Oligodendrocyte transcription factor 2;
OoC	Organ-on-a-chip
OTX2	Orthodenticle homolog 2
PBS	Phosphate Buffer solution
PCL	Polycaprolactone
PDMS	Polydimethylsiloxane
PDO	Polydioxanone
PFA	Polyformaldehyde
PLGA	Poly(lactic-co-glycolic acid)
PTFE	Polytetrafluoroethylene
qRT-PCR	Quantitative real time-Polymerase Chain Reaction
RA	Retinoic acid
RG	Radial glia
RNA-seq	RNA sequencing
ROCK	Rho-associated protein kinase
RT	Room temperature
SAG	Smoothened agonist
SB	SB431532
SEM	Scanning electron microscope
SF	Silk-fibroin
SHH	Sonic hedgehog
SLA	Stereolithographic
SOX2	SRY-Box Transcription Factor 2
SVZ	Subventricular zone

TGF-β	Transforming growth factor-β
Triton X-100	TX 100
VZ	Ventricular zone
Wnt	Wingless-related integration site family

List of tables

Table 1. A summary of the main papers in the field of BoC 20
Table S1. Primary antibodies used for brain organoid immunostaining. 69

List of figures

Figure 1. 1 11
Figure 1. 2 12
Figure 1. 3 16
Figure 1. 4 17
Figure 1. 5 18
Figure 1. 6 21
Figure 1. 7 22
Figure 3. 1 27
Figure 3. 2 31
Figure 3. 3 32
Figure 3. 4 33
Figure 4. 1 37
Figure 4. 2 38
Figure 4. 3 39
Figure 4. 4 40
Figure 4. 5 41
Figure 4. 6 42
Figure 4. 7 43
Figure 4. 8 43
Figure 4. 9 44
Figure 4. 10 45
Figure 4. 11 46
Figure 4. 12 47
Figure 4. 13 48
Figure 4. 14 49
Figure 4. 15 50
Figure 6. 1. 58

Figure S1....70
Figure S2....71
Figure S3....71
Figure S4....72
Figure S5....72
Figure S6....72
Figure S7....73

1. Background introduction

1.1 Cerebral Organoid

The human brain is one of the most complex organs in the animal kingdom. In an adult brain, there are over ten billion of neurons and glial cells that form over 60 trillion neuronal connections, making it very difficult to study *in vitro*[1]. However, the recent investigation of human embryo stem cells (hESCs) differentiation *in vitro* has provided new opportunities for researchers. hESCs can generate all cells of the three germ layers allowing for the creation of complex multicellular cultures from a single cell source[2]. The 3D floating cultures of ESC aggregates, also known as embryo bodies (EBs), have been demonstrated to maintain significant cell pluripotency[3] and could be induced into differentiated 3D models that mimic human brain development[4]. Further studies proved that Matrigel (MG)[5], a solubilized basement preparation extracted from the Engelbreth-Holm-Swarm (EHS) mouse sarcoma, which is rich in extracellular matrix (ECM) proteins, could be used to provide crucial cues for the self-organization of the neuroepithelium *in vitro*[6]. When the neuronal-induced EB was embedded in MG, a spherical structure with large neuroepithelia buddings was obtained, which contained multiple neural stem and progenitor cells (Figure 1.1) and could be further differentiated into cerebral organoids[7].

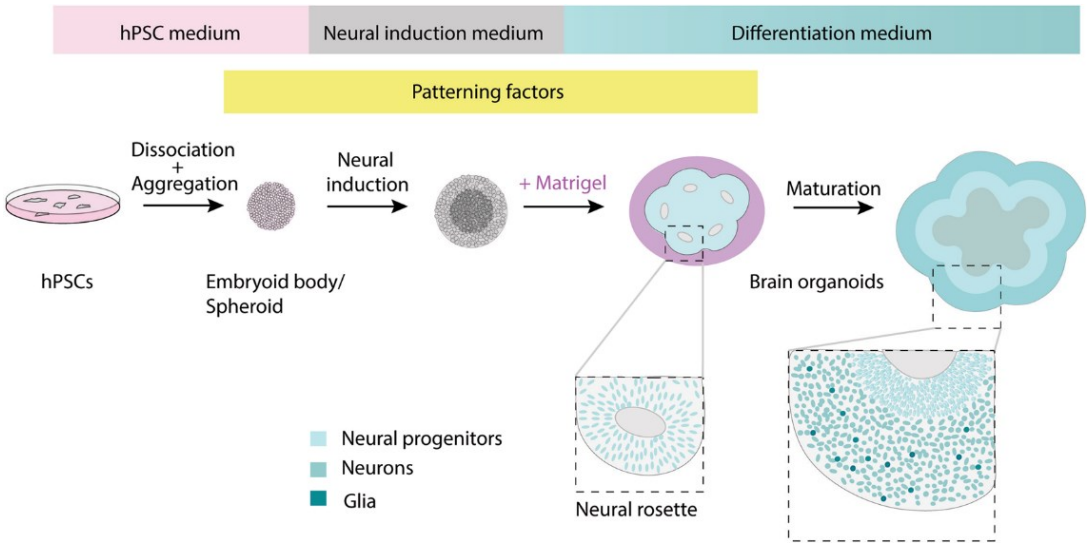


Figure 1. 1. Schematics of cerebral organoid culture procedures, adapted from Sidhaye et al.[8]

A cerebral organoid was first reported by Lancaster et al. in 2013[9]. In their protocol, EBs were formed with the aggregation of hESCs in the 96 U-bottom well under low-

adhesion culture conditions. Neural basal media containing N-2 and B-27 was used to induce the formation of neuroectoderm with spontaneously established apicobasal polarity. Based on previous studies[10, 11], N-2 is a serum free additive that supports the expression of primary neuroblastomas and post mitotic neurons originating from the peripheral and central system. B-27, as widely cited additive for neuronal cell culture, is used for supporting the survival of embryonic, postnatal, adult hippocampal, and other central nervous system (CNS) neurons. After MG embedding and further culture, large buds of neuroepithelium that contained fluid-filled cavities resembling brain ventricular zones could be obtained (Figure 1.1). The cortical layers resembling the developing brain could be observed through immunostaining and sketched as Figure 1.2B. Such a self-sorted structure recapitulated many features of the early human brain during embryonic development, including cytoarchitecture, cell diversity, and maturation. The apical-basal polarity of radial glia (RG) progenitors, interkinetic nuclear migration, division modes of neural stem cells, and the pattern of neuron migration that represent the major features of developing cortex were also well maintained in a brain organoid[2, 12].

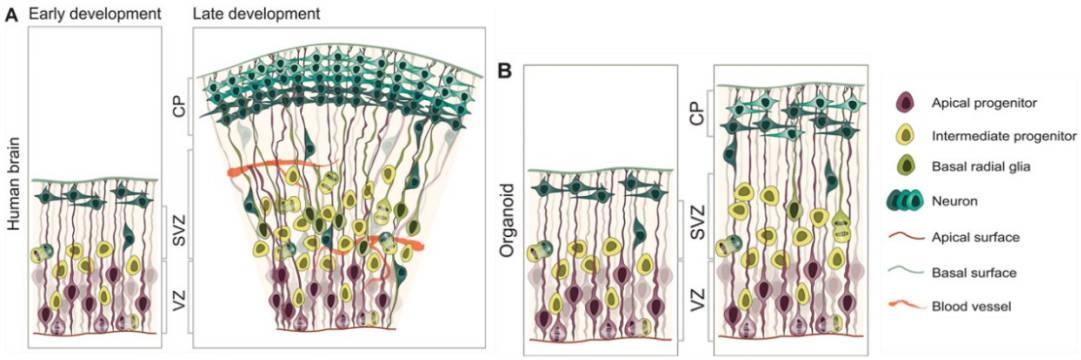


Figure 1. 2. A) *In vivo* human brain cortical layer structure for both early and late development. **B)** Cell arrangement in human brain organoid with an irregular pattern and the absence of blood vessel. Adapted from Kelava et al.[2] CP is short for cortical plate. SVZ is short for subventricular zone. VZ is short for ventricular zone.

Morphologically, the human brain divides into multiple regions, including the forebrain, midbrain, and hindbrain. In each region, the cortical plate is responsible for controlling multiple sensory functions and contains six layers of neuronal cells with blood supply (Figure 1.2A). Compared to the cortical plate in the early human brain, the neural ectoderm surface of the brain organoid (Figure 1.2B) displayed a similar but irregular cell arrangement[2]. Such a layering structure was still rudimentary. Luckily, significant improvement in 2016 by Qian *et al.* has enabled the generation of neurons corresponding to all six layers[13]. They developed a miniaturized spinning bioreactor

system and improved the culture media based on previous monolayer studies. Cellular diversity of the cortex was maintained in their cortical organoids generating various types of RG cells and neurons, recapitulating the cytoarchitecture of the developing cerebral cortex. These studies have demonstrated the great potential of brain organoids as they could be advanced via engineering platform to model the cortical structures of the developing brain with considerable accuracy[2].

Functionally, excitatory and inhibitory neurons in brain organoids were also identified by multiple experiments and could reflect the development and maturation of the brain during embryonic stages[14]. RNA sequencing (RNA-seq) or single cell RNA-seq[15], are highly advanced tools for profiling the global gene expression of large populations of individual cells, to which the related studies have indicated that the brain organoids also showed remarkably high similarity to the developing brain at the transcriptomic level[16]. The same level of similarities in cell type, structure, and function to the developing brain have never been reported in other models besides brain organoids, making them revolutionary *in vitro* brain models[14].

1.2 Applications of cerebral organoids

Brain organoids, derived from pluripotent stem cells, can be used to elucidate species-specific properties[17, 18]. In 2016, Otani et al. compared the induced pluripotent stem cells (iPSC)-derived organoids from human, chimpanzee and macaque and revealed the different proliferative dynamics of neural progenitors that led to different neurogenesis outputs, explained the neocortical size differences among primates[19]. Therefore, the methodology of brain organoids offered new access to comparative experiments across species and could facilitate our understanding of human evolution via studying the neocortex development. Additionally, brain organoids could also provide human-specific models that help reduce the usage of animal models in biological studies.

Since the inaccessibility of the human brain has been initially overcome with brain organoids, neurodevelopmental brain disorders are now extensively explored *in vitro*. In 2018, Lin et al. introduced an isogenic APOE4 brain organoids via CRISPR/Cas9 genome editing from iPSCs to interrogate the pathological mechanism of Alzheimer's disease (AD), as APOE4 is the most significant genetic risk factor for AD[20]. They revealed that converting APOE4 to APOE3 could trigger multiple AD-related pathologies. Other examples shed light on congenital diseases such as microcephaly. During the Zika virus outbreak in South America, human iPSCs-derived brain organoid

models were widely used to study the pathology of Zika virus infection, as considerable newborn microcephaly has been found related to the virus[21, 22]. Lancaster et al. have interrogated microcephaly with patient-derived organoids and RNA interference technology to determine the pathogenic role of CDK5RAP2[9]. These examples proved the combination of genetic manipulation with brain organoid as an unprecedently powerful tool in disease modeling, which led to further clinical applications such as high-throughput drug screening and toxicity examination[23].

1.3 Limitations of brain organoids

Although brain organoids provided unique access to brain modeling and great flexibility to be induced and differentiated, several limitations blocked their broad application in biomedical engineering researches. First, the lack of vasculature could lead to inner apoptosis and limit the size and long-term culture of brain organoids due to the restricted mass transport of oxygen and nutrients with passive diffusion[2]. Brain organoids have been engrafted into the brains of living mice to obtain an integrated vascular structure with such an *in vivo* vasculature system. The vascularization was proved to enhance the maturation of brain organoids. However, as this method was dependent on *in vivo* transplantation, the convenience and reproducibility of an *in vitro* model was lost[24]. Other studies have reported the incorporation of vascular components such as endothelial cells and mesenchymal stem cells within the brain organoids, where the vascularization was only achieved on the surface of the brain organoid[25]. Engineering approaches are currently seeking to achieve an inner channel that allows nutrient transport to replace natural vascularization, which broadens the methodology for long-term organoid culture, and has become an important study direction in the field of brain organoid direction[26].

Second, the brain organoid is an incomplete neural system. Many neural cell types that are not differentiated from neuroectoderm are still absent, such as microglia, endothelial cells, hematopoietic cells, and meninges[14]. In this case, the brain organoid could not appropriately simulate the interactions with non-neural cells. Furthermore, the immaturity of brain organoid has made it challenging to study late-onset and age-dependent diseases of the CNS[27], such as Miller–Dieker syndrome, a severe form of lissencephaly, since current organoids cannot form cortical folds. Therefore, to simulate age-dependent neurodegenerative disease, induced aging in the brain organoid via pharmacological or genetic methods is required[28]. But it is questionable whether such induced aging events accurately mimic the natural aging process *in vivo*.

Finally, a brain organoid that goes through unguided differentiation of the pluripotent stem cells lacks a polarized and predictable anatomy that faithfully mimics the developing brain[29]. Although the cortex layers of brain organoid are well organized, the representative brain regions are randomly structured, which hinders the reproducibility of brain organoids and limits their application value. Natural human brain development is regulated by multiple biomolecular factors that determine the differentiation and regionalization of all kinds of cells. Previous studies on ESCs differentiation in 2D cultures have identified the major signaling pathways related to CNS development[4, 30]. Based on this information, several methodologies have combined signaling modulators and growth factors to induce brain organoids to differentiate into specific brain regions[31], including dorsal and ventral cortex[32], choroid plexus[33], retina[34, 35], midbrain[21], cerebellum[36], and spinal cord[37]. These region-specific brain organoids have provided reproducible models for the studies of specific brain regions. Afterwards, a novel methodology that fused region-specific organoids together to generate a polarized complex called “assembloid”[38] has emerged as a popular topic in developing reproducible topography of the *in vitro* brain model and allowed for the modeling of cellular interactions between different brain regions.

1.4 Assembloids

In 2017, Bagley *et al.* developed dorsal cortex organoids and ventral organoids and co-embedded them in MG (Figure 1.3A)[39]. The two separate organoids fused within one week and showed functional connectivity with interneurons migration. In their results, the dorsoventral cell-cell interactions were exhibited by the migration, morphology modification, and synapses formation of γ-aminobutyric acid(GABA)–ergic cortical interneurons and cortical glutamatergic neurons, thus generating a functional neural circuit modeling the developing brain. It was claimed that the assembloids were invaluable tools reflecting the interactions between specific brain regions through long-distance cell projections, thus illustrating the basic mechanisms of brain formation in utero[40].

The assembly of dorsal and ventral brain organoids has inspired other combinations of region-specific organoids following the rules of brain development. For example, the striatum-midbrain assembloids could be used to model the cortico-spinal projections[41]. With genetically edited chromosomes, such assembloids can be used to investigate the cortico-striatal pathway and how its defects lead to neuropsychiatric disease. Andersen et al. explored the potential of assembloids in establishing an

anteroposterior axis[42] by fusing cortical spheroid with spinal cord spheroid and achieved a functional multi-synaptic circuit *in vitro*. Corticofugal neuron projection, motor neuron connection, and further contraction of 3D muscles were observed from the cortical-spinal cord assembloids.

Nowadays, as shown in Figure 1.3B, the fusing of brain organoids has become an important methodology in investigating the interactions between brain organoid and other cell-based objectives, including different region-specific brain organoid and 2D differentiated cells originating from CNS system. These cells worked as functional units to elucidate the effect of different cells on the developing brain. For example, microglia-like cells have been integrated into the cortical organoids and generated the main component in amyloid plaques, the β-amyloid protein, and subsequently have been used to model AD[20].

Therefore, the methodology of assembloids significantly expanded the complexity and application versatility of the brain organoids. And in terms of generating reproducible anatomy, the assembloids containing two different brain regions shed light on a significant advancing direction in this field, leading to a polarized CNS axis that more comprehensively mimics the natural brain. Furthermore, for being easy to operate, the assembloids have become one of the most important tools on brain organoid polarization studies.

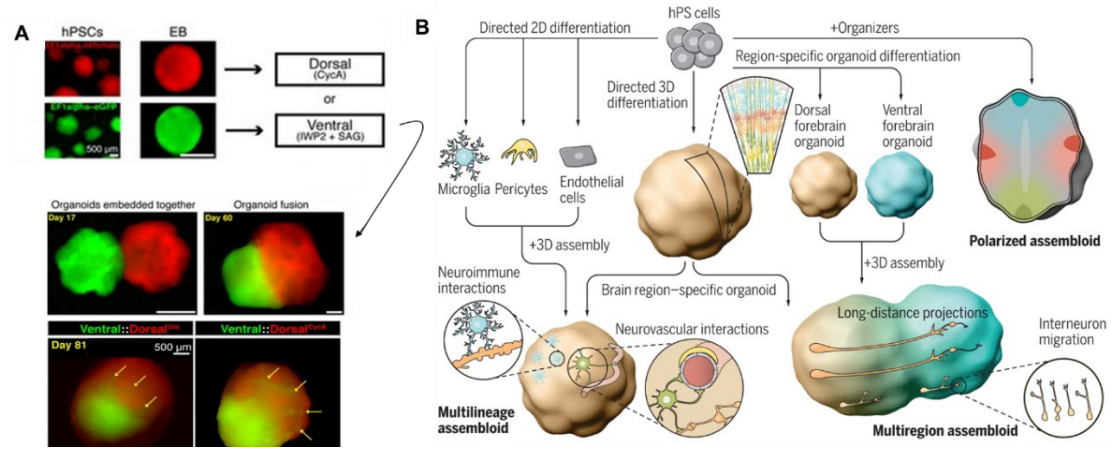


Figure 1. 3. A) Fused dorsal-ventral organoids showing the migration of interneurons. Scale bars = 500 µm. Adapted from Bagley et al.[39] **B)** Schematics of the formation of multilineage assembloid and multi-region assembloid. Adapted from Pasca et al.[38]

Polarized brain organoids hold great promise for simulating the functional connectivity and the complex circuitry of the brain, as compared to the commonly used cortical cerebral organoids[42]. However, such unnatural fusion process of assembloids

is not ideal, as it potentially hinders the complex developmental process of neural tube polarization and brain regionalization *in vivo*[39]. To address this issue, currently, researchers are seeking methods to generate polarized brain organoids by taking inspiration from the natural events.

1.5 Brain regionalization and brain organoid polarization

The development of CNS in mammals starts with the enclosure of a neural plate and subsequentially forms a tubular structure known as the neural tube (Figure 1.4A). In the third week of gestation, three vesicle structures appear along the neural tube and further develop into the forebrain, midbrain, and hindbrain respectively[43]. The division of neural tube into these primary brain vesicles along the anteroposterior axis is mainly mediated by Wingless-related integration site family (Wnt) signals[44]. Simultaneously, the neural tube undergoes dorsoventral polarization under the guidance of Bone morphogenic protein (BMP) and sonic hedgehog (SHH) signals (Figure 1.4B[45]). These biomolecules, known as morphogens, are secreted from respective signaling centers and form corresponding concentration gradients that regulate subsequent gene expression and cell differentiation[46]. The spatial arrangement of the differentiated cells will guide the neural tube polarizing into different brain regions in a concentration-dependent manner.

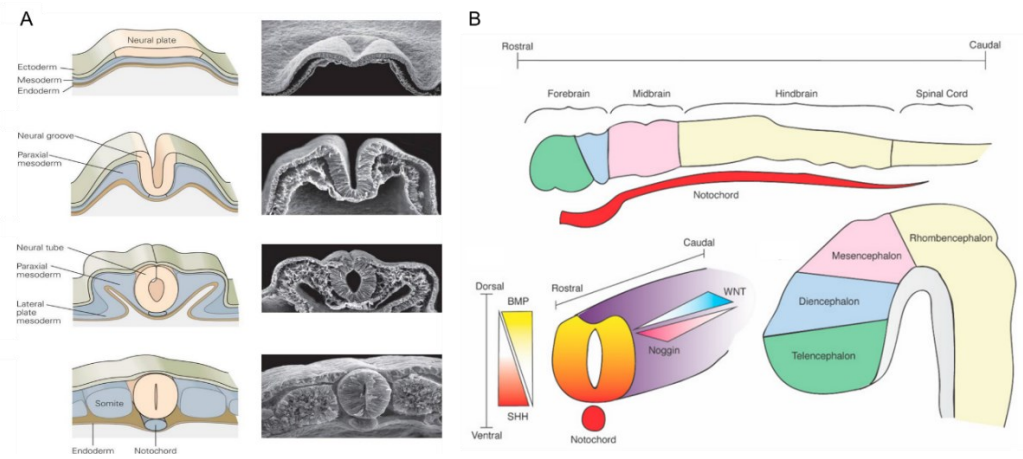


Figure 1. 4. A) Schematics and scanning electron microscope (SEM) images of the neural plate folding and closing process during embryo development, reproduced from neupsykey.com. **B)** Schematics of *in vivo* neural tube polarization along both anteroposterior and dorsoventral axes, coordinated by Wnt-Noggin signal and the BMP-SHH signal, reproduced from Brady et al.[45]

The first molecule identified as a morphogen was the *bicoid gene* product, which is essential for anteroposterior neural tube patterning in *Drosophila* embryos[47]. Based on the "source and sink" model that Francis Crick proposed in 1970, many groups have

attempted to analyze and visualize the formation of morphogen gradients in a quantitative manner, and illustrate the concentration-dependent cell differentiation events[48]. Wolpert's French flag model that explained the mechanism of such concentration effect has been extensively used in developmental studies[49]. It is now believed that the number of ligand-receptor interactions determines the subsequent downstream signaling and gene expression[50, 51].

Many studies have demonstrated the caudalization effect of the Wnt signaling pathway on a stem cell level. Dual SMAD inhibition (dual SMADi) and Wnt activation-based regulatory methodologies are primarily utilized in mediating hESCs neuronal caudalization[52, 53]. In 2020, Libby et al. used the Wnt signal activator, CHIR99021 (CHIR), to treat human iPSCs to generate brain organoids and found the amazing extension within two weeks of culture that recapitulated neural tube axial elongation in the early development (Figure 1.5A, 1.5B)[54]. Spatial representative identities have been marked on the anteroposterior axis with the Homeotic (HOX) gene family (Figure 1.5C[54]), which proved the significant potential of human iPSCs in modeling neural tube caudalization via primary specification of progenitors. Similar research conducted by Girgin et al. reported a system deriving axial elongation via the aggregation and pre-treatment of mouse ESCs[55]. The culture media contained Transforming growth factor-β (TGF-β) activator and the serum-free ectoderm induction factors was proved to promote the ESCs aggregation and obtained epiblast identity and stimulated axial elongation without using Wnt.

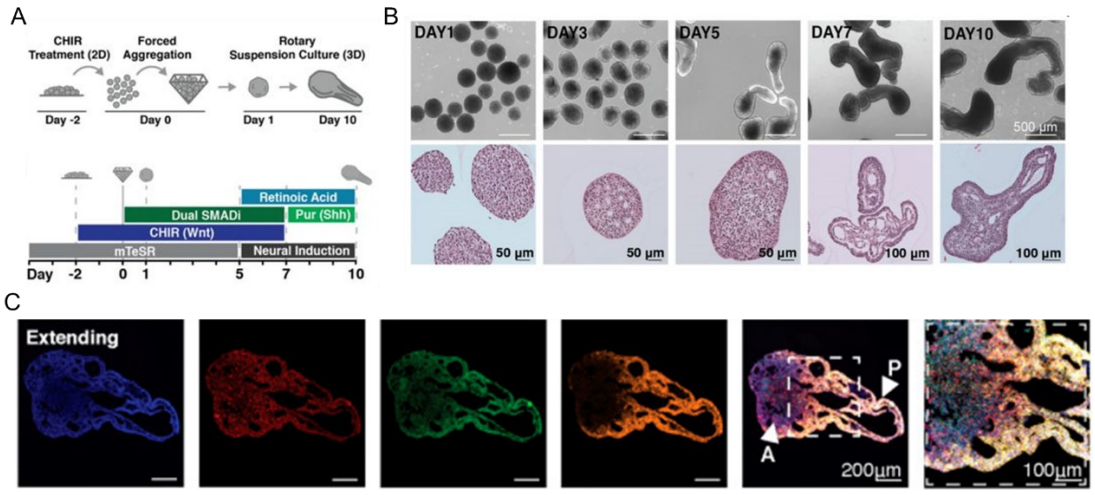


Figure 1. 5. A) Schematics of experimental set-up. **B)** BF (top) and histological (bottom) images of the Wnt treated brain organoids. **C)** RNA-scope of sectioned elongated organoids with probes for HOX genes (DAPI: blue; *HOXB1*: red; *HOXC6*: green; *HOXB9*: orange) marking different regions of the spine on day 10. Arrowheads mark anterior (A) and posterior (P) ends of organoids. Adapted from Libby et al.[54]

These studies enhanced our understanding of the complex regulatory networks during early brain development and provided insights into establishing the EB axis *in vitro*. However, these models still failed to provide an ideal polarized differentiation of brain organoids due to the lack of a natural Wnt gradient environment.

In 2019, Cederquist et al.[56] introduced a method by fusing a cluster of SHH-secreting cells on one side of the forebrain organoid, subsequently formed a SHH concentration gradient via passive diffusion. As a result, organoid dorsoventral polarization was observed with immunostaining to identify different spatial markers, which proved the biophysical gradient paradigm could be applied in brain organoid polarization study. Their achievement provided an example of morphogen concentration gradient-mediated brain organoid polarization. However, the Wnt signal concentration gradient guiding brain organoid anteroposterior polarization has not been achieved yet, thus leaving a blank space illustrating brain regionalization *in vitro*.

1.6 Microfluidic gradient generator

Microfluidics refers to the technology involving chip systems that use microchannels with a size of tens to hundreds of microns to manipulate microflows. The microscale channels provide unique fluid phenomena that enable a series of micromachining and microoperations that are difficult to complete by other bioengineering methods[57]. Nowadays, microfluidic devices have been widely used in biomedical researches due to their advantages in boosting high-throughput drug screening and disease modeling[58]. In tissue engineering, the culture of organoids with a microfluidic chip was known as an organ-on-a-chip (OoC) system, which has already been developed for the lung, liver, kidney, intestine, heart, bone marrow, skin, and brain[59]. These systems offered the advantages of precise control for many kinds of stimuli during organoid culture and analysis, including biochemical, electrical, and mechanical stimuli. On the other hand, microfluidic devices have also been used to address the limitations of blood supply to improve the long-term survival of organoids[26].

For brain-on-a-chip (BoC) systems especially, there has been significant momentum in recent years. As Table 1 displayed[60], different microfluidic chip designs could provide flexible and versatile bioengineering operations on brain organoid culture, thus enabling multiple topics of research that broadly expanded the field of brain organoid studies. These previous works demonstrated that BoC systems held great promise in controllable exposure of growth factors, including the morphogens mentioned in section 1.5, which altered the model of brain organoid cultures to a certain extend.

Besides bioengineering manipulation, BoC systems have also been used in disease modeling. For example, Nishida et al. reported neural stem cell spheroids could be integrated into microfluidic chambers and used as simple brain models for the study of AD[61]. But until now, the utility of microfluidic devices in brain organoid polarization has never been reported.

Cell type	Flow	Chip	Topic
hiPSCs	Manually changed media	Micropillar array (PDMS)	*In vivo* organogenesis[62]
hiPSCs	Syringe pump	PDMS chip	Prenatal nicotine exposure[63]
hiPSCs	Peristaltic pump	Resin chip	Brain organoid formation[64]
hiPSCs	Rocking platform	PDMS chip	Human brain development[65]
hESCs	Manually changed media	Based on a tissue culture dish	Wrinkles appearance[66]
hESCs	Manually changed media	Chip array	Prenatal exposure to cannabis[67]
hESCs	Rocking platform	Tubular chip	Neuroinflammation[68]
hESCs	Acoustic flow	Clear resin device	Growth of human brain organoids[69]

Table 1. A summary of the main papers in the field of BoC. Adapted from Saorin et al.[60]

In 2019, Rifes et al. used a microfluidic platform with sequential mixing channels to generate linear concentration gradients of glycogen synthase kinase 3 inhibitor (GSK3i)[70], which is a Wnt signal activator, also known to induce ESCs differentiation into progressively caudalized neural fates (Figure 1.6A, 1.6B). They demonstrated the microfluidic GSK3i gradient could induce anteroposterior polarization of a monolayer culture of hESCs. The rostral neural gene indicator OTX2, which covers the entire fore- and midbrains *in vivo*[71], has shown a decreased expression (Figure 1.6C) along the imposed GSK3i gradient. By day 14 of culture, they divided the monolayer cultures into

five regions and reported that the boundary between the expression of OTX2 and GBX2, where the midbrain-hindbrain boundary (MHB) arises during development, was consistently located between the third and fourth regions. These results firmly indicated the polarization of neural stem cells along the anteroposterior axis of the neural tube.

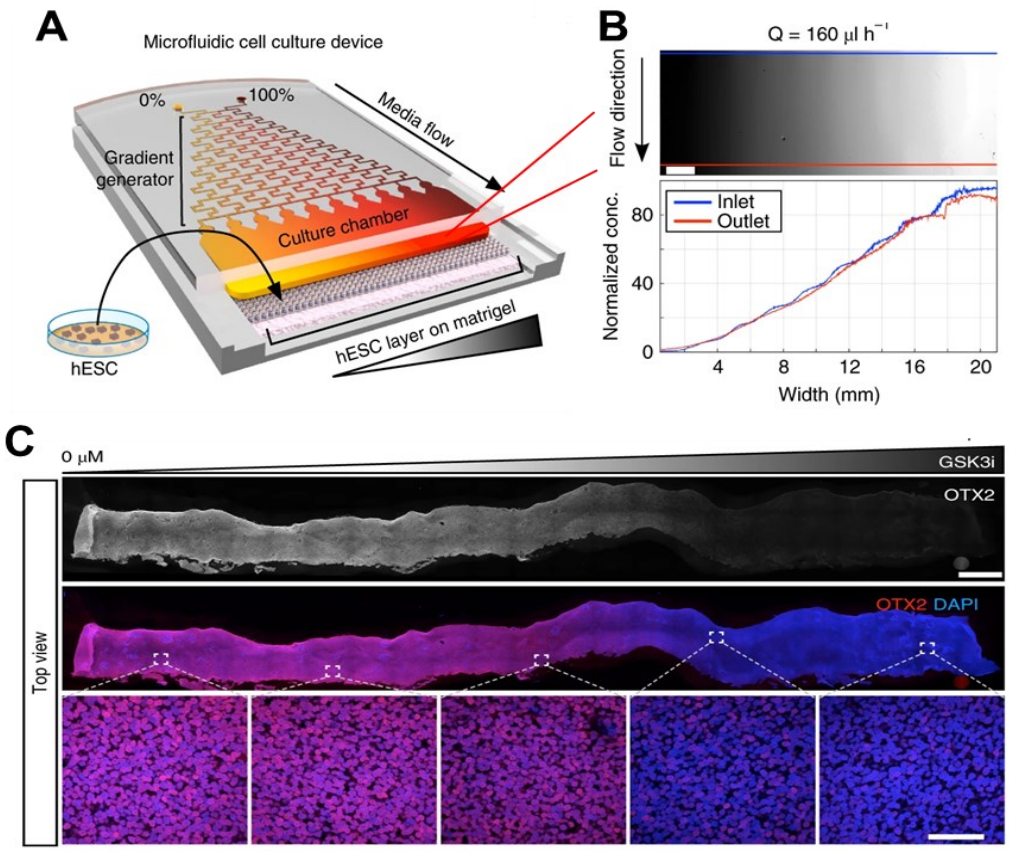


Figure 1. 6. A) Schematics of the microfluidic gradient generator with a hESC layer in the culture chamber. **B)** Concentration gradient visualization and the quantification profile showing a linear increase of the fluorescent signal. **C)** The whole-mount staining of the cells in the culture chamber with a decreased OTX2 (red) expression. Scale bars are top 1 mm and bottom 100 µm. Adapted from Rifes et al.[70]

We believed a microfluidic gradient generator would be a powerful tool to apply external morphogen concentration gradients mimicking *in vivo* neural tube polarization conditions for inducing brain organoid polarization. Based on Rifes' research, the questions remaining are how to assemble the brain organoid in such a microfluidic chamber, and how to reconstruct the shape of the brain organoid to accommodate the microfluidic platform.

1.7 Scaffold mediated brain organoid

The use of 3D biomaterial to support and guide tissue growth is a common strategy in tissue engineering[72]. Recent studies have utilized this strategy for organoid generation, which provided a promising tool to increase the reproducibility of brain organoids[73, 74]. In organoid studies, scaffold was referred to as the biocompatible material of any shapes and properties that was embedded with cell suspension to allow the growth of regulated 3D structures[75]. As for brain organoid, in 2017, Lancaster et al.[76] used poly(lactic-co-glycolic acid) (PLGA) microfilaments to support the attachment of hESCs and generated brain organoids with enhanced neuroectoderm formation and cortical development (Figure 1.7A, 1.7C). The scaffolds could largely increase the interaction surface, subsequently facilitated the nutrient exchange efficiency and expanded the growth space of the brain organoids (Figure 1.7B). They observed that the linear scaffold-guided brain organoids grew into a more complex topography than the round organoids derived from spherical EBs. Moreover, genetic quantification analysis of the material-guided organoids from different batches displayed highly reproducible results in terms of neuroectoderm formation, while the spheroids were variable as usual.

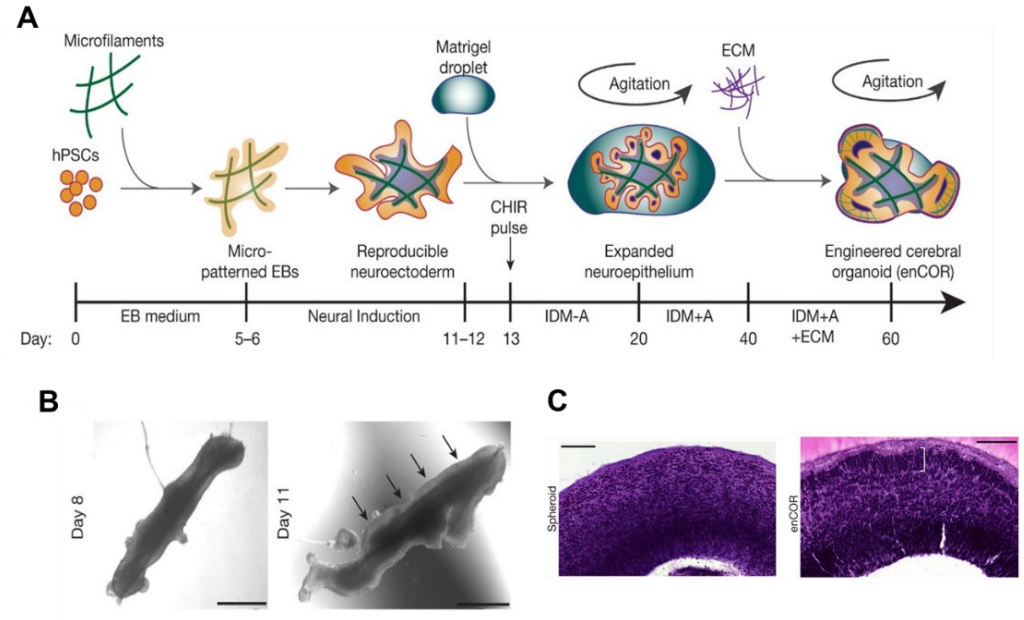


Figure 1. 7. A) Schematics of the procedure of generating scaffolds-guided brain organoids. **B)** BF images for the engineered cerebral organoids (enCOR) on day 8 and 11. Scale bars are 250 μm. **C)** Histological staining by H&E for both spheroid organoid and the enCOR on day 60. The radially oriented cortical plate in the enCOR was much denser than that in the spheroid organoid. Scale bars are 100 μm. Adapted from Lancaster et al.[76]

In the presented study, regarding of reconstructing the shape of brain organoids to fit in the microfluidic gradient generator mentioned in section 1.6, biocompatible materials with high tensile strength and are easy to handle would meet the demands.

Traditionally, polycaprolactone (PCL) is a synthesized biodegradable material with various applications in tissue engineering and long-term drug delivery[77, 78]. It has also been utilized in tumor organoid studies[72], demonstrating that the 3D-printed PCL scaffold facilitated cancer stem cell enrichment and could also be used to study drug resistance in cancer treatment. Another example was reported in 2021, when Rothenbucher et al. demonstrated the use of PCL scaffolds could grow brain organoids with a flattened morphology[79], expanded the exploration on brain organoids reconstruction. These researches proved the biocompatibility of PCL to support brain organoid growth.

The commonly used PCL scaffold material was fabricated by electrospinning, which led to a micro-scaled fiber that was easy to degrade[80-82]. The micro-PCL scaffold for brain organoid culture was fragile and difficult to handle and transfer, which was not suitable for the microfluidic design mentioned in section 1.6. PCL suture thread circulating on the market, on the other hand, has the perfect size and strength to support an elongated brain organoid generation assembled in the 2 cm wide microfluidic culture chamber. The suture threads are very cheap and easy to obtain, which have the potential to be alternative scaffold materials in regulating simpler brain organoid morphologies.

Suture threads can be divided into two categories based on their properties: absorbable suture threads and unabsorbable suture threads. The absorbable suture threads are referred to as materials that degrade under the skin and lose most of the tensile strength in 60 days, normally with great biocompatibility and can be further categorized into natural material suture threads and polymer synthesized suture threads[83]. For natural material, catgut has the longest history in medicine, and was manufactured by collagen matrix from the submucosal layer of the sheep intestine[84]. The absorption time of catgut is very short, only 4 to 5 days after surgery. However, it has the disadvantages of insufficient tension, difficulty in suturing and knotting, body rejection reaction, poor adaptability *in vivo*, and rapid loss of tensile strength in digestive fluid and infection environments.

Silk suture thread, another type of natural absorbable sutures, holds advanced compatibility with human tissue and is less likely to cause allergic reactions and inflammatory reactions[85]. On the other hand, silk sutures have high tensile strength

and wear resistance, which can provide sufficient support to promote wound healing. Last but not least, silk sutures are easy to thread and allow accurate operation. Silk-fibroin (SF) is the main protein that silk suture is composed of, and is one of the strongest fibers and has a similar tensile strength compared to glass fiber[86]. The chemical properties of SF have proven to be versatile for a wide range of bioengineering applications, including drug delivery and regenerative medicine of cardiac, blood vessel, and bone[87, 88].

For chemical synthesized suture thread, polydioxanone (PDO) is one of the most commonly used materials, possesses high tensile strength and stability. It is a semi-crystalline polymer that can be manufactured via an extrusion process that allows controllable shaping and prevents spontaneous depolymerization. In medical cosmetology, PDO has been used as lift thread material that could be buried under the skin and hydrolyzed and degraded after six months[89]. As medical implants, studies with PDO as tissue engineering scaffolds were also widely reported, including the application in bone, dental, or ligament/tendon repair, based on its stiffness and biodegradability[90].

Regarding the demand for the microfluidic chip design in section 1.6, the length of the brain organoid would be stretched to 2 cm long, which is considerably larger than any scaffold-mediated brain organoids reported before. Until now, the combinations of scaffolds with brain organoids were only experimented with micro-scaled materials, focusing on the minor disturbance and potential chemical interactions between material fibers and the brain organoids. Contrarily, the minimal diameters of suture threads range from 0.07 mm to 0.4 mm, allowing brain organoids to grow around them into a big entity[91]. The suture thread mediated brain organoid with a large size would be an unprecedented example in this field. Different sizes of suture threads would provide possibilities for investigating the influence of scaffold diameters on brain organoid growth. The potential of the reconstruction of brain organoid morphology by using suture threads has yet to be verified.

2 Hypothesis, aims and objectives

Based on the literatures mentioned above, the main hypothesis of this project is the microfluidic gradient generator and commercial suture threads can be used to develop a culture platform inducing elongated brain organoid anteroposterior polarization. If proven, this work will provide a powerful methodology in the field of brain organoid, which can also be used to interrogate the unresolved mechanisms underlying the cell fate decisions and spatial organization of the development of human CNS.

The specific aims and objectives can be summarized as follow:

1) Establish an engineering platform consisting of the in-house microfluidic gradient generator and an elongated brain organoid culture regime, and verify the concentration gradient generated in the organoid chamber via fluorescent indicator and live cell microscopy.

2) Determine optimal rostral/caudal morphogen exposure plans for both short-term and long-term culture accommodating the microfluidic anteroposterior patterning paradigm using traditional round brain organoids.

3) Achieve brain organoid elongation with commercial suture threads (PCL, PDO and silk) with different sizes, and prepare suitable cell crowns for the microfluidic chip assembly.

4) Perform brain organoid anteroposterior polarization experiment via the microfluidic platform and verify the main hypothesis.

3 Material and methods

3.1 Microfluidic gradient generator

3.1.1 The microfluidic chip and cell crown design

The microfluidic gradient generator includes two inlet reservoirs, multiple mixing channels with a cross-section of 200 x 200 μm (width x height), a culture chamber (20 x 10 x 4 mm) for organoid assembly with two slopes on the side, and an outlet reservoir (Figure 9A). The Autodesk Computer Aided Design (Auto CAD) (Solidworks) file was provided by Dr. Richard Wang, which is a negative mold for the positive polydimethylsiloxane (PDMS) chip casting. To support the elongated organoid growth, a cell crown with two clamping clips (Figure 9A) was designed by Dr. Richard Wang and Dr. Ruoxiao Xie. It is to stretch the tissue engineering scaffold and fit it in the microfluidic culture chamber. It can also be kept in 6 well plates for the still culture condition before or after microfluidic gradient exposure.

3.1.2 PDMS microfluidic chip and cell crown fabrication

The CAD-designed file for the microfluidic chip was transferred into stl. format, and then printed via PrusaSlicer v2.5.0 for Prusa SL1S 3D printer. The orange tough commercial resin (Prusa) was used with 0.025 Ultra Detail as printing precision. After printing and isopropanol absolute (IPA) washing with sonication for 15 mins, the mold was cured with 4 h UV exposure at 60°C. Then the mold was left in a 60°C oven overnight, and treated with O_2 plasma (1 mBar, 0.6 W, 5 min) to obtain a negatively charged surface. Trichloro(1H,1H,2H,2H-perfluorooctyl)silane (Sigma-Aldrich 448931-10G) was used for the silane anti-adhesion layer treating for the mold for 4 h in the desiccator.

PDMS and the curing agent (SYLGARD® 184 Sylgard 184 Elastomer Kit, VWR 634165S) were mixed with a 10:1 mass ratio and degassed by 1000 rpm centrifuge before being poured into the mold. The mold filled with PDMS mixture was put into the desiccator for 30 mins vacuum degassing to remove the air bubbles entirely. Afterwards, the mold with PDMS was moved into a 60°C oven for curing for 2 h. PDMS chip demolded from the negative mold was O_2 plasma treated together with a clean glass slide (VWR MARI1120090091) for 1 min (1 mBar, 0.6 W). Then the two surfaces bonded with positive and negative charge attraction.

The cell crown and clips were printed by an SLA 3D printer (Formlabs Form2) with a proprietary biocompatible resin (Formlabs RS-F2-BMCL-01) to allow biocompatibility during cell seeding and organoid growth. Both were cleaned with IPA under sonication and cured with 4 h UV light at 60°C before use.

3.1.3 Brain organoid culture within the microfluidic chip

Customized glass plates with screw holes were used to clamp the PDMS-glass microfluidic chip (Figure 3.1A). Polytetrafluoroethylene (PTFE) tubing with I.D. × O.D. 0.5 mm × 1.0 mm (Sigma-Aldrich Z609706-1PAK) was used for inlet and outlet media flow (Figure 3.1B). Before assembly, the microfluidic chip, clamping plates, screws, and nuts were autoclaved. The tubing was washed with ethanol and rinsed with phosphate buffer solution (PBS) 3 times, then exposed to UV light for 30 mins. The syringes filled with media were pre-warmed in the 37°C incubator overnight to remove air bubbles. During assembly, the cell crown with/without elongated organoid was put in the culture chamber. The top clamping glass plate was then pressed to seal the PDMS surface, ensuring no leakage. After the bottom plate was assembled with all screws and nuts, pre-warmed syringes were connected by the tubing.

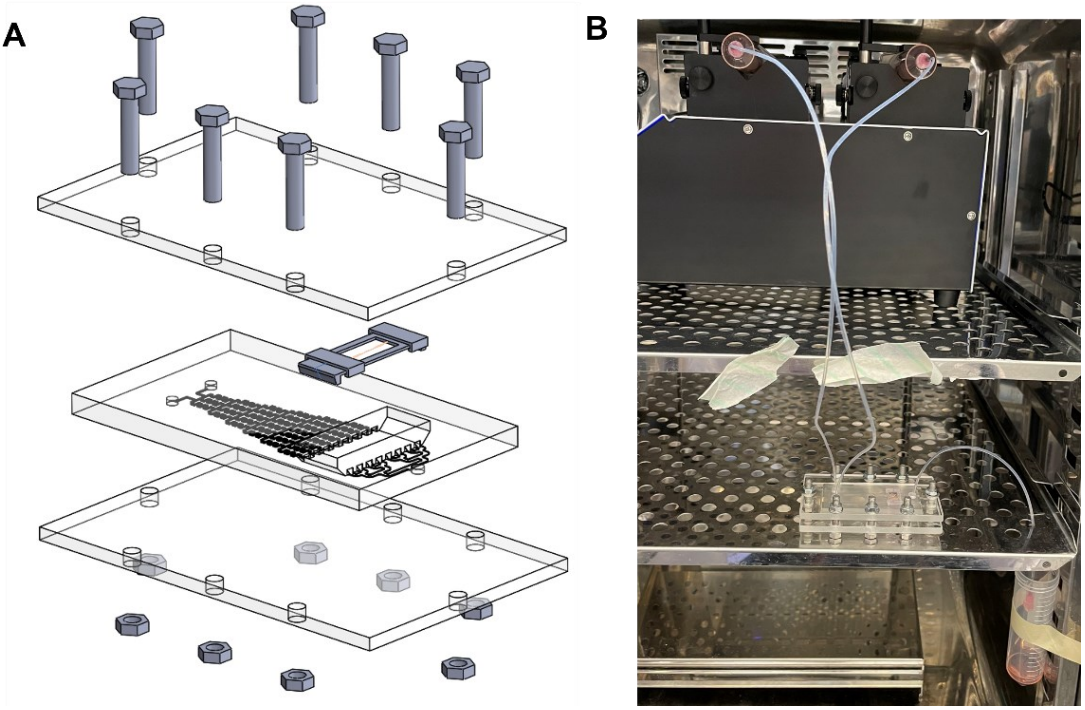


Figure 3. 1. **A)** Schematics of microfluidic gradient generator assembly with cell crown, clamping plates, screws and nuts. The graph was provided by Dr. Richard Wang. **B)** Picture of the organoid patterning platform in a 37℃ CO_2 incubator.

To fill the micro-channels and culture chamber with media, the syringes were purged manually until all air was removed. The whole set (Figure 9B) was moved into the 37 °C incubator and connected to the syringe pump (Harvard Apparatus 33DDS). To fully maintain the concentration gradient in the culture chamber and prevent air bubbles formation, the flow rate was decelerated gradually as follows: 1 mL/min 1 min, 500 μL/min 2 mins; 300 μL/min 2 mins; 100 μL/min 2 mins; 50 μL/min 2 mins; 30 μL/min 2 mins; 10 μL/min 2 mins; 5 μL/min 10 mins, and 1.33 μL/min as final flow rate, which provided 160 μL/h media supply for organoid growth.

3.1.4 Gradient visualization

Following the microfluidic chip operation protocol in 3.1.3, red food dye (Sigma-Aldrich 458848-100G) or 2.5 μM fluorescein sodium salt (FSS) (Sigma-Aldrich F6377-100G) in Dulbecco's modified Eagle's medium (DMEM) was added to one of the syringes recapitulating the 100% morphogens which regulate organoid polarization. The red food dye was used to directly visualize the gradient formation in the channels and chamber in the preliminary experiment stage, while the fluorescent signal of FSS can be detected with a live cell imaging platform (Zeiss AxioScope Observer) and be monitored overnight. The concentration gradient in the culture chamber was analyzed by ImageJ quantitively. Gradient detection and data analysis were performed by Dr. Richard Wang and Dr. Ruoxiao Xie.

3.2 Round cerebral organoid cultivation

3.2.1 Organoid culture media

Stem cell media: mTeSR Plus (STEMCELL 100-0276) media with 50 μM rho-associated protein kinase (ROCK) inhibitor (Selleck Chemicals S1049) and 1% (v/v) Penicillin/Streptomycin (Invitrogen).

Neural induction media: DMEM/F23 (Gibco) with 1% (v/v) Penicillin/Streptomycin, 1% (v/v) N-2 supplement (Invitrogen 17502048), 1% (v/v) GlutaMAX supplement (Invitrogen), 1% (v/v) MEM-NEAA (Invitrogen) and 1 μg/mL heparin (Sigma, H3149). Filtered before use.

Improved - A media: 1:1 (v/v) mixture with DMEM/F12 and Neurobasal media (Gibco) with 1% (v/v) B-27 minus vitamin A supplement (Invitrogen, 12587010), 0.025% (v/v) insulin (Sigma, I9278), 0.5% (v/v) N-2 supplement, 1 mg/mL sodium bicarbonate (Sigma-Aldrich S5761-500G), 1% (v/v) GlutaMAX supplement (Invitrogen), 1% (v/v)

Penicillin/Streptomycin. Filtered before use.

Improved + A media: 1:1 (v/v) mixture of DMEM/F12 and Neurobasal media with 1% (v/v) B-27 supplement (Invitrogen 17504044), 1% (v/v) vitamin C solution (350 mg/ 50 mL DMEM/F12), 1% (v/v) GlutaMAX supplement, 0.5% (v/v) N-2 supplement 0.025% (v/v) insulin, 1% (v/v) Penicillin/Streptomycin and 1 mg/mL sodium bicarbonate. Filtered before use.

3.2.2 H9 cell maintaining

Human embryo stem cell line H9 was obtained from WiCell and maintained with feeder-free conditions. hESC qualified MG (Corning 354277) was used and diluted with DMEM/F12 according to manufacturer's instructions, hereinafter referred to as "coating MG". 1 mL coating MG solution was used to coat each 6 well plate at 37°C incubator for over 45 mins, and was removed before cell seeding. 2 mL mTeSR Plus was added to each well and exchanged daily. At 60 ~ 70% confluency, cells were passaged by ReLeSR (STEMCELL 05872) treatment for 3 mins at 37°C incubator, collected with 1 mL mTeSR Plus for splitting.

3.2.3 Cerebral organoid cultivation

For cell seeding, H9 cells with 60% confluency were detached by ReleSR and collected with 1 mL stem cell media as described in 3.2.1, centrifuged with 800 rpm for 5 mins. The supernatant was removed. Cells were resuspended with stem cell media to ensure 9000 cells per 150 µL for each well in the round bottom 96 well plate (Ultra-Low Attachment, Scientific Laboratory Supplies, 444-1020). On day 3, 150 µL mTeSR Plus media was changed by multi-channel pipettes. On day 5, day 7, and day 9, media was replaced by 150 µL neural induction media as described in 3.2.1 to regulate the neural fate differentiation of the EBs. On day 10 ~ 13, optical clearing organoid borders were observed. In this stage, organoids were embedded with MG (Corning 356235) droplets on a parafilm for gel formation in the 37°C incubator for 30 ~ 45 mins. Neural induction media was continually used to flush the droplets off the parafilm and maintain organoids growth in the 6 cm petri dish. 2 ~ 3 days after the MG embedding, Improved - A media was used for organoid maturation and exchanged every 2 ~ 3 days. On day 17 ~ 18, organoids were placed on an orbital shaker at a speed of 57 rpm. The short-term culture terminated on day 20, and the organoids were fixed by 4% polyformaldehyde (PFA) (Sigma-Aldrich). The long-term culture for more mature organoids terminated on day 40, during which the media was replaced by Improved +A on day 25 and exchanged every other day.

3.3 Brain organoid elongation

3.3.1 Material biocompatibility examination

Silk fiber from Cambridge collaborators, 20G PCL (DHGate), PDO suture thread (DHGate), and 27G PDO suture thread (Private pharma SKU240) were cut into small fragments and sterilized with 2% (v/v) Penicillin/Streptomycin in PBS overnight. Before cell seeding, all materials were coated with coating MG with 1% (v/v) Penicillin/Streptomycin for at least 1 h. During cell seeding, silk fiber fragments were mixed with cell suspension with stem cell media to ensure 18000 cell/well with 150 µL media for the U-bottom 96 well plate. For the suture thread fragments, after cell seeding with 18000 cell/well with 150 µL media, the materials were moved manually by autoclaved tweezers to ensure 1 or 2 fragments in each well. The following culture protocol was consistent with the conventional cerebral organoid culture protocol and was terminated on day 20. Bright field (BF) images were taken every other day with triplicates to demonstrate organoid viability, attachment, and growth.

3.3.2 Organoid elongation with 27G PDO

To regulate hESCs around the scaffold surface and facilitate cell attachment, before sterilization, an agarose (Sigma-Aldrich) base was made, fitting corresponding cell crown with 27G PDO scaffold (Figure 3.2). Briefly, 3% (w/v) agarose in PBS was prepared and warmed up by microwave. Cell crown-PDO scaffold was merged with 1.5 mL agarose solution in 6 well plate. After gelling, the cell crown-PDO scaffold was removed, and the groove for cell suspension was cut to 2 mm wide with a blade along the mark left with the 27G PDO thread. Both the agarose base and cell crown-PDO scaffold were sterilized with 2% (v/v) Penicillin/Streptomycin in PBS overnight. Before cell seeding, the scaffold was coated with coating MG with 1% (v/v) Penicillin/Streptomycin, and the agarose base was pre-diffused with mTeSR Plus media with 1% (v/v) Penicillin/Streptomycin for 2 h. Ultra Low attachment 6 well plate (VWR 734-1582) was used to set the agarose base and the cell crown-PDO scaffold.

60% confluent H9 cells were detached with ReleSR and suspended with stem cell media to obtain high cell density of $2*10^7$/mL. 80 µL cell suspension was added to each scaffold ensuring all cells were regulated in the groove. After standing for 30 mins, 1.5 mL stem cell media was added slowly to the surface of the agarose base for nutrient supply. On day 2, the cell crown-PDO scaffold with organoid attached was lifted with a tweezer and removed to the sterilized holder, which was 3D printed by biocompatible

resin (Figure 3.2) as well. On day 11, PDO scaffold with elongated brain organoid was removed from the cell crown and set on a hydrophobic parafilm for MG embedding. After gelling, the organoid embedded in MG was flushed off by neural induction media for further culture. The media supply protocol maintained the same as conventional cerebral organoids, and the experiment terminated on day 20.

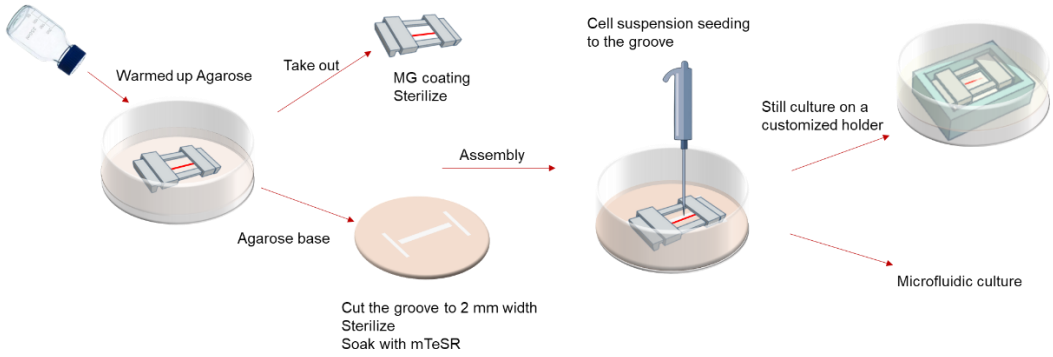


Figure 3. 2. Schematics of elongated organoid seeding process with 27G PDO scaffold.

3.3.3 20G PDO/PCL-guided elongated organoid

2 cm PDO/PCL 20G suture threads were sterilized with 2% (v/v) Penicillin/Streptomycin in PBS and coated with MG as described in section 3.3.1. A customized PDMS holder was demolded from an orange tough resin 3D printed mold and sterilized with 2% (v/v) Penicillin/Streptomycin in PBS overnight. A 4 well ibidi chip was pre-coated with Anti-Adherence Rinsing Solution (STEMCELL 07010) and then washed with PBS before seeding. 1 mL cell suspension with density of $4.8*10^5$/mL was added to the ibidi well together with the scaffold. On day 2, the scaffold with a thin layer of cells was moved to the PDMS holder for further culture. On day 11, the scaffold with organoid was moved to hydrophobic parafilm for MG embedding, and the media supply was consistent with the conventional cerebral organoid protocol. The experiment was terminated on day 20.

3.4 Anteroposterior microfluidic patterning

Andersen's protocol (Figure 3.3A, and B) was used to generate caudal identity of the brain organoids[41]. Based on that, an optimized anteroposterior patterning protocol for microfluidic settings was determined as shown in Figure 11C for 20-day short-term culture by the following experiments. For dual SMADi treatment, Andersen et al used dorsomorphin (DM) and SB431532 (SB), while the most common protocol is the

combination of SB431532 and Noggin (NG)[92, 93], of which the stock in-house was sufficient. In our experiment (Figure 3.3C), NG was used instead of DM.

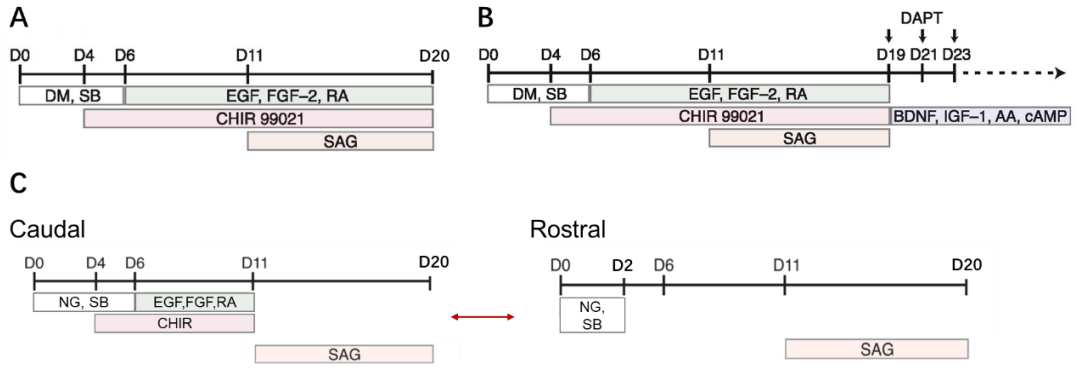


Figure 3. 3. Andersen's protocol[41] for **A)** short-term and **B)** long-term spinal cord spheroids culture. **C)** Time scale of caudal and rostral organoid protocols for the microfluidic platform. The concentrations of the above factors are: Noggin Fc 100 ng/mL (R&D System 719-NG-050), SB431532 10 μM (Tocris 1614), EGF 20 ng/mL (R&D System 236-EG-200), FGF2 20 ng/mL (R&D System 233-FB-025/CF), RA 10 nM (Sigma-Aldrich R2625-50MG), CHIR99021 3 μM (Miltenyi Biotech CT99021), smoothened agonist (SAG) 0.1 μM (Cambridge Bioscience Ltd (Cayman Chemical) CAT11914-1), brain-derived neurotrophic factor (BDNF) 20 ng/ml (Peprotech 450-02), Insulin-like growth factors -1 (IGF-1) 10 ng/ml (Peprotech 100-11), L-ascorbic acid (AA) 200 nM (Wako 321-44823), cyclic adenosine monophosphate (cAMP) 50 nM (Sigma-Aldrich D0627) and DAPT 2.5 μM (STEMCELL technologies 72082).

Briefly, after cell seeding with 27G PDO scaffold, the cell crown-scaffold-organoid assembly was removed from the agarose base and settled into the autoclaved microfluidic chip as described in 3.1.3. The microfluidic culture chamber was filled with media containing the gradient of morphogens as shown in Figure 3.4. Since the brain organoid spontaneously differentiates towards a rostral fate, only one side of the inlet was supplied with caudalization factors, including CHIR, retinoic acid (RA), fibroblast growth factor (FGF), and epidermal growth factor (EGF). After morphogen gradients exposure for 9 days, on day 11, the scaffold-organoid was taken out and embedded with MG, then set on the customized holder for further cultivation and characterization.

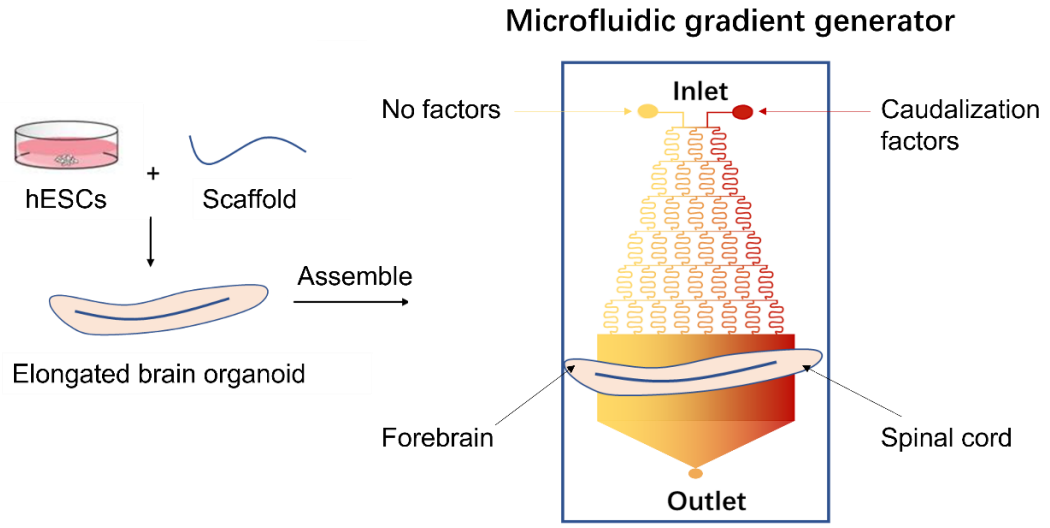


Figure 3. 4. Schematics of the microfluidic gradient generator guided brain organoid polarization. With forebrain identity on the side without morphogen treatment, and spinal cord identity on the opposing side, a continuous and polarized brain organoid along the anteroposterior axis shall be obtained.

3.5 Brain organoid characterization

3.5.1 Cryosection

The organoids fixed on day 20/40 by 4% (w/v) PFA/PBS were washed with PBS 3 x 15 mins and dehydrated by 30% (w/v) sucrose (Merk 84097-250G)/PBS overnight at 4 °C. O.C.T. matrix (Sakura 4583) was used for organoid embedding under -80 °C in the cryomolds (25 x 20 x 5 mm, Agar Scientific AGG4580). 20 µm tissue slices were obtained with a cryostat machine (Cryostar NX70) at -12°C and collected with Microscope slide Superfrost Plus adhesion (Fisher Scientific 10149870), stored at -20 °C freezer for further staining.

3.5.2 Organoid sections immunostaining.

For immunostaining, slides were soaked in PBS at room temperature (RT) for 10 mins to remove the water-soluble O.C.T. matrix. Organoid sections were post-fixed with 4% (w/v) PFA/PBS for 5 mins, then washed for 3 x 15 mins with PBS. Afterwards, organoid sections were permeabilized and blocked with 0.3% (v/v) Triton X – 100 (TX 100) (Sigma Aldrich X100-100ML) and 5% (w/v) Bovine albumin (BSA) (Millipore Sigma 10735078001) in PBS for 30 mins at RT. Primary antibodies were diluted accordingly with 5% (w/v) BSA and 0.1% (v/v) TX100 in PBS, as described in Table S1. 400 µL diluted primary antibody solution was added to each slide overnight at 4°C

in a humidified box. The slides were washed 3 x 15 mins with PBS-T (PBS + 0.01% (v/v) TX100), and 400 µL 1:500 diluted secondary antibodies (Alexa fluor) was added to each slide for 2 h at RT in a dark humidified staining box. Afterwards, 400 µL 1:1000 diluted DAPI (2 mg/mL stock, BD 564907) solution was added to each slide and incubated for 5 mins. The slides were washed 2 x 15 mins with PBS-T and 1 x 15 mins with PBS. Fluorescence mounting medium (DAKO s3023) was used to fix the cover slides before imaging.

3.5.3 Confocal microscopy imaging

Images were acquired by Leica SP8 confocal microscopy with 405 nm diode laser for DAPI, 488 nm argon laser (GFP), 543 nm HeNe laser (Alexa Fluor-543/555), and 633 nm HeNe laser (Alexa Fluor-633-647). 10X and 20X images were taken in triplicates for each sample and processed with Fiji ImageJ.

3.5.4 RNA extraction

For homogenization, organoids on day 20/40 were torn by P10 tip pipetting vigorously and washed with PBS, centrifuged at 800 rpm to remove the embedded MG. Discarding the supernatant, cell suspension was lysed with TRIZOL reagent (Life Technologies 15596026), and kept in -80°C freezer overnight. 1 mL TRIZOL reagent was used to homogenize four 20 day-organoids and two 40 day-organoids. 0.2 mL chloroform per 1 mL TRIZOL reagent was added for phase separation and vortexed vigorously for 15 s, incubated at RT for 3 mins. Samples were centrifuged at 12000 g for 15 mins at 4°C. A clear aqueous phase with RNA was collected in 1.5 mL Eppendorf (EP) tube. Then, RNA was precipitated with 500 µL isopropyl alcohol per 1 mL TRIZOL reagent used for the initial homogenization. Samples were incubated at RT for 10 mins and centrifuged at 12000 g for 10 mins at 4°C. The supernatant was removed, and the RNA pellet on the bottom was washed twice with 1 mL 75% (v/v) ethanol, and centrifuged at 7500 g for 5 mins at 4°C. Removing the supernatant entirely, the RNA pellet was left still and dried at RT for 30 mins and dissolved with Nucleus free water. The RNA concentration was measured by Nanodrop with A260/280 ratio < 1.6. Samples were stored at -80°C for cDNA reverse transcription.

3.5.5 cDNA reverse transcription

According to the RNA concentration of samples, following the protocol of QuantiTect® Reverse Transcription kit, 1 µg RNA was reverse transcribed to cDNA in 20 µL reactions. The concentration of cDNA was calculated by Nanodrop with

A260/280 ratio < 1.8. Samples were stored at 20°C for quantitative real time-Polymerase Chain Reaction (qRT-PCR).

3.5.6 qRT-PCR

Calculating and ensuring 10 ng cDNA/10 µL reaction, Taqman primer probes and Taqman MasterMix were used following the TaqMan® Multiplex PCR Optimization protocol. qRT-PCR was performed with a Vii6 PCR system with the following cycling conditions: 20 s at 95 °C, 40 cycles of 1 s denature at 95 °C, and 20 s of extending at 60 °C. Taqman probes of *HOXA2* (Thermo Fisher 4331182), *HOXC6* (Thermo Fisher 4331182), *HOXC9* (Thermo Fisher 4331182) were used to demonstrate the rostral-caudal identity. Relative gene expression to mean ± standard error of mean (S.E.M.) was an average of four replicates and was normalized using $2^{-\Delta Ct}$ method to *GAPDH* gene (Thermo Fisher 4331182) expression.

3.6 data analysis

Statistical analyses were performed with GraphPad Prism 7.0. The results were presented as the means ± S.E.M. One-way ANOVA (analysis of variance) and Sidak's test was used for comparison among multiple groups for a certain gene expression. '*' indicates p value < 0.05, '**' indicates p value < 0.01.

4 Results

4.1 Specific aims

As mentioned in section 2, 4 specific aims were included in this project.

For the first aim, the brain organoid polarization platform was primarily established, as described in section 3.1.1 ~ 3.1.3. Optimizations on the chip design were performed to obtain a consistent concentration gradient in the culture chamber, which was visualized with FSS and ImagJ as described in 3.1.4.

For the second aim, as Andersen's caudalization protocol provided multiple combinations regarding the concentration of different morphogens, the one that generated spinal cord identity was chosen in this project, as described in section 3.4 (Figure 3.3A and B), and was verified with round organoids first. Based on this, modifications to the morphogen exposure periods were performed with traditional round brain organoids to obtain optimal rostral/caudal patterning protocols that were suitable for the microfluidic anteroposterior patterning paradigm.

For the third aim, silk fiber, 20G PCL, 20G, and 27G PDO commercial suture threads were selected as candidate materials. Material screening was performed with round brain organoids as described in 3.3.1 to verify the biocompatibility. Cell crown, scaffold holders were designed for elongated brain organoids fixation and culture, as described in section 3.3.2 and 3.3.3.

For the fourth aim, a comparison experiment was conducted with 27G PDO elongated brain organoids under still or microfluidic culture conditions to exclude the influence of microfluidic shear stress on brain organoid growth. On the other hand, the determined rostral/caudal patterning protocols were verified with 20G and 27G PDO elongated brain organoids separately. Finally, the brain organoid anteroposterior polarization experiments were performed via the microfluidic platform with 27G PDO suture threads. 20G PDO suture threads could also be used in the future.

4.2 Microfluidic concentration gradient generator

4.2.1 Microfluidic chip characterization and optimization

The microfluidic brain organoid patterning platform was prepared according to

section 3.1.1~.3.1.3. In such design, a low Reynolds number (Re) (0.0023) and a Peclet number (Pe) > 1 (2.19) for the fluorescent additives were calculated by using the following equations:

$$Re = \frac{\rho v L}{\mu} \qquad (1)$$

$$Pe = \frac{uL}{DB} \qquad (2)$$

Where ρ is the density of media, v/u is the local flow velocity, L is the characteristic linear dimension, μ is the dynamic viscosity coefficient of media at 305 K, and D_B is the mass diffusion coefficient of the media[94]. This result indicated the flow was dominated by laminar flow and advection in the culture chamber.

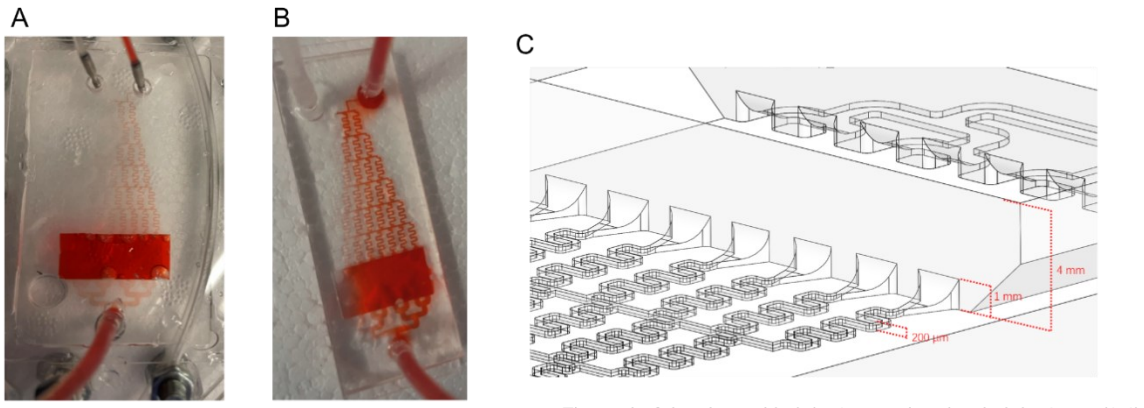


Figure 4. 1. A) and **B)** compared the microfluidic chips with different channel width and chamber height, where gradients were indicated with red food dye. **C)** Design of slop structures at the end of the microchannels.

To prevent microbubble formation and obtain a stable chamber gradient, the microfluidic chip design underwent multiple modifications. Initially, the microchannel with a height of 200 μm was too small compared to the chamber with a height of 4 mm, leading to the failure of the gradient formation in the chamber, visualized with red food dye(Figure 4.1A). However, a testing chip with a chamber of 2 mm in height and channels of 400 μm in height was able to maintain the chamber gradient stably (Figure 4.1B). Based on this observation, slope structures (Figure 4.1C) with open ends of 1 mm in height were added to the end of the channels, which decreased the height difference and facilitated the stability of gradient in the chamber.

4.2.2 Microfluidic gradient visualization

The optimized chip was examined with FSS indicator and live cell microscopy overnight. As shown in Figure 4.2A, two sufficiently mixed laminar flows in the microchannels and a clear gradient formed in the culture chamber (Figure 4.2B) were observed. The ImageJ quantification result revealed a gradually increased fluorescent signal in the direction perpendicular to the microflows while remaining stable in the direction parallel to the flows. Such results indicated the optimized microfluidic platform was ready to be used for the subsequent experiments with elongated brain organoids.

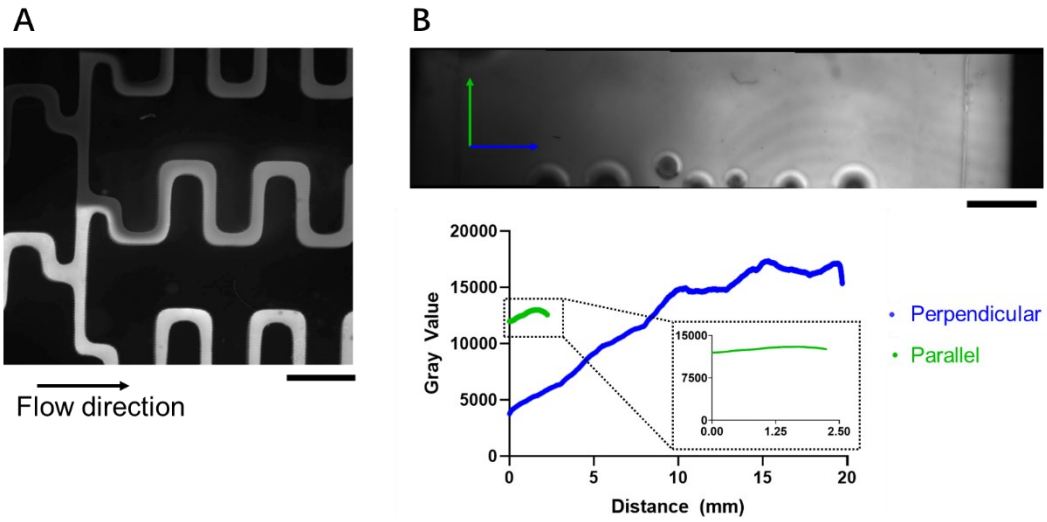


Figure 4. 2. A) FSS indicated laminar flows mixing in the microfluidic channels under live cell microscopy. Scale bar = 1 mm. **B)** Live cell image showing the fluorescent signal in the culture chamber (up, scale bar = 1 cm) and ImageJ quantification analysis (bottom) for both directions perpendicular and parallel to the flow. The images and analysis result were provided by Dr. Richard Wang and Dr. Ruoxiao Xie.

4.3 Caudal and rostral protocol for microfluidic patterning

4.3.1 Short-term culture

The feasibility of using Andersen's protocol[41] (Figure 3.3A) in generating 20 day caudalized brain organoids was verified. The BF results (Figure 4.3A) showed the cauldalized organoids were bigger than conventional cerebral organoids, and maintained well-regulated lumen regions surrounding the core area resembling cell self-sorting and neuroepithelium formation. The neural stem cell marker SOX2 was expressed with both 20 day-control and caudalized organoids, while the caudal marker GBX2 was only observed in the caudalized organoids (Figure 4.3B). This result

suggested the caudalized organoids were successfully generated. However, this protocol requires the addition of the caudalization morphogens from day 0 to day 20, which is not a realistic time point for starting the microfluidic gradients as H9 cells will not be able to attach to the scaffolds on day 0. To adapt Andersen's protocol to our microfluidic platform, optimizations are demanded in terms of the timing of the caudalization morphogens exposure.

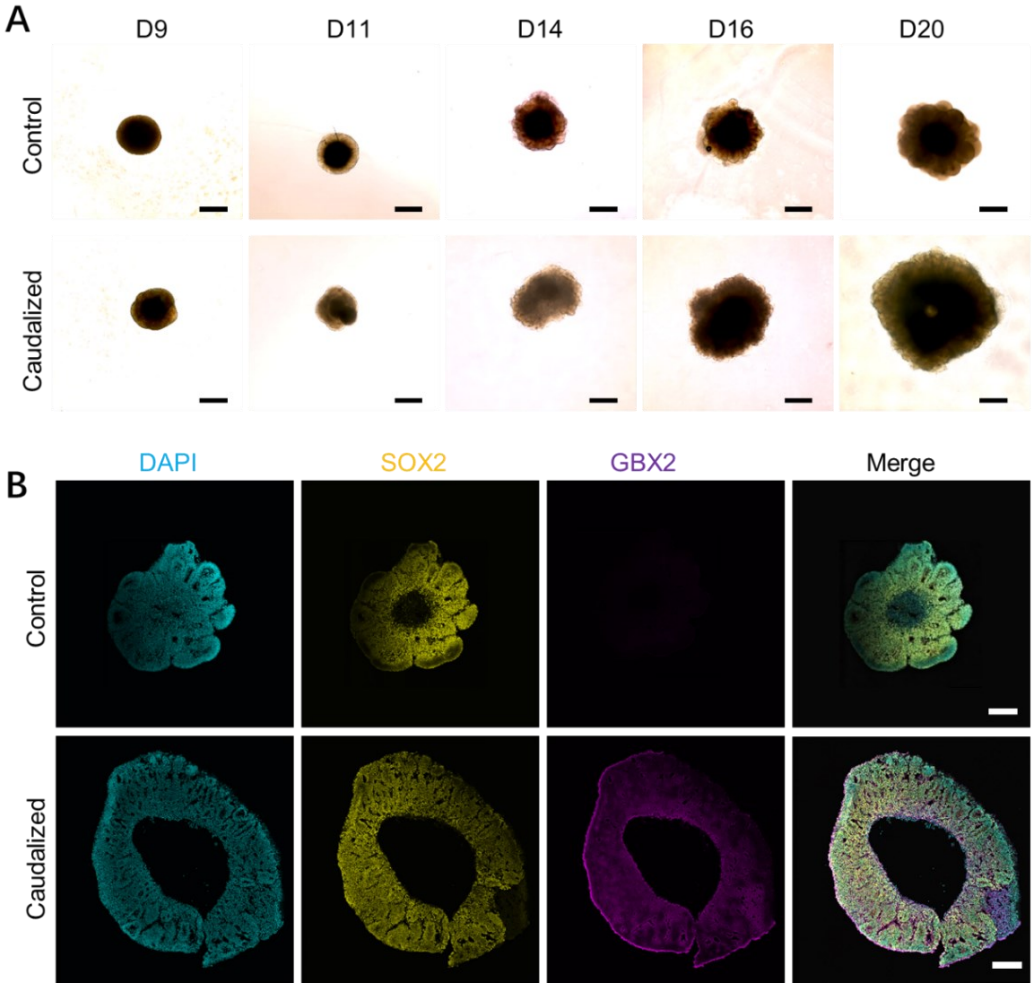


Figure 4. 3. A) BF images showing the growth of control and caudalized organoids following Andersen's protocol. **B)** Immunostaining images indicating the expression of SOX2 and GBX2 of both 20 day-control and caudalized organoids. Scale bars = 500 μm.

To ensure cell attachment for at least 2 days prior to microfluidic patterning stimuli, and to avoid interference with the gradient diffusion caused by MG embedding on day 11, the supply of caudalization factors: CHIR, RA, FGF2, and EGF was limited from day 2 to day 11. To determine the best protocol for microfluidic anteroposterior patterning, four groups of experiments were conducted as listed in Figure 4.4. The

concentrations of all factors were consistent with section 3.4 (Figure 3.3). Conventional round organoids were used to test all the conditions. qRT-PCR and immunostaining were used to find the optimal condition, which would be applied to the scaffold-guided elongated organoids and the microfluidic patterning procedure subsequently.

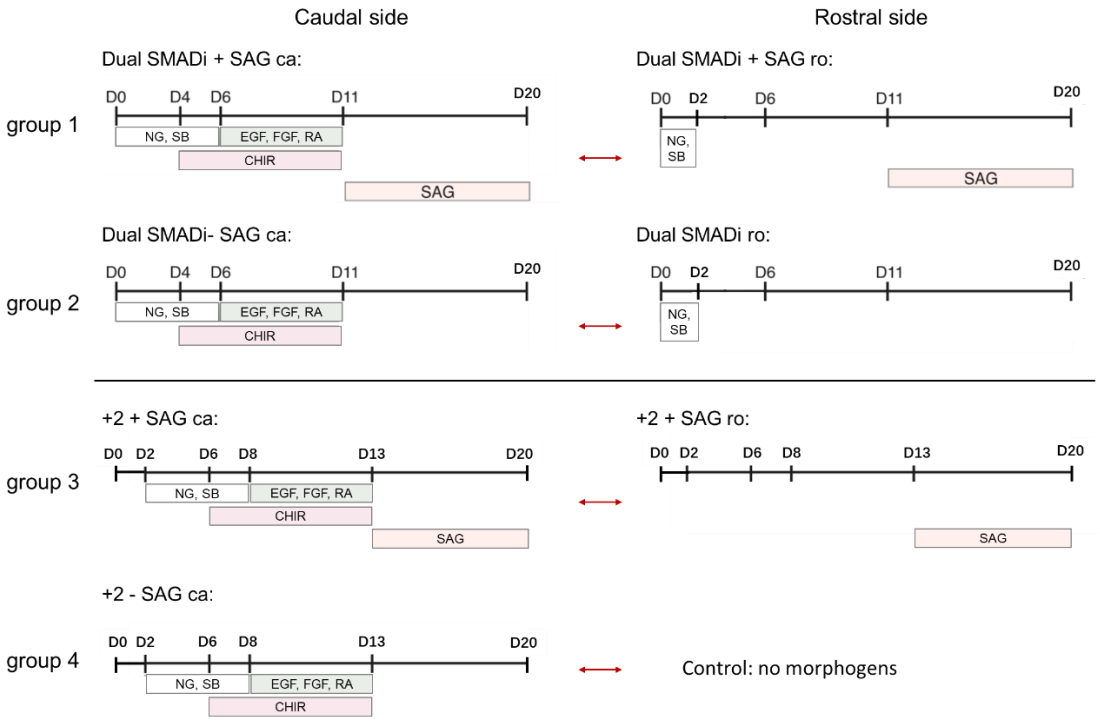


Figure 4. 4. Caudal and rostral protocols for round organoid preliminary experiments. The terms: "Dual SMADi + SAG ca", "Dual SMADi + SAG ro", "Dual SMADi - SAG ca", "Dual SMADi - SAG ro", "+2 + SAG ca", "+2 + SAG ro" and "+2 - SAG ca" were continually used in the following text. "ca" and "ro" refer to the caudal group and rostral group respectively. For group 1 and 2, MG embedding was performed on day 11. For group 3 and 4, MG embedding was performed on day 13.

The expression of neuron marker MAP2, caudal marker GBX2, and motor neuron marker OLIG2 that expressed in human spinal cord region, were examined by immunostaining and confocal microscopy (Figure 4.5, S1). All groups expressed MAP2, indicating that they have maintained neural identity. For the caudal groups, OLIG2 expression was only observed in the "Dual SMADi + SAG ca" organoids, which also managed to maintain the conventional organoid morphology as shown in Figure 4.5 and Figure S1.

Figure 4.5 also suggested that for the caudal groups, the use of dual SMADi in the first two days was essential, as without it, thick neuron layers and random organoid structures were observed with or without SAG supplement (+2 + SAG ca; +2 - SAG ca). For the rostral groups, dual SMADi in the first two days induced neuron layers

around the organoids (Dual SMADi + SAG ro; Dual SMADi - SAG ro). But adding SAG after MG embedding resulted in a more regulated organoid structure, indicating that SAG may play a role in cell sorting and organization.

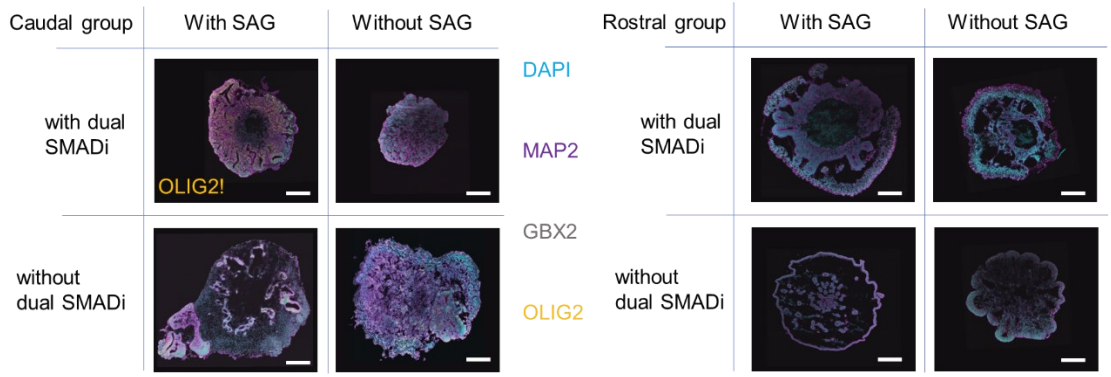


Figure 4. 5. Immunostaining summary for organoids with modified protocols on day 20. The merged images included DAPI (cyan), MAP2 (magenta), GBX2 (grey), OLIG2 (yellow). With/without dual SMADi refers to the treatment condition from day 0 to day 2. With/without SAG refers to the treatment condition from day 11 to day 20. Scale bars = 500 μm.

The organoids derived from original Andersen's caudalization protocol and all the modified conditions were further examined with qRT-PCR (Figure 4.6A). The rostral groups: control, Dual SMADi + SAG ro, Dual SMADi - SAG ro, +2 +SAG ro, had no expressions of the spinal cord-related genes: *HOXC6* and *HOXC9*, and the expressions of hindbrain related gene HOXA2 were considerably low. In contrast, all the caudal groups have maintained hindbrain and spinal cord identity, indicating the modifications of the caudal factors (CHIR, RA, EGF, FGF) exposure period did not interfere with the caudal identity of the brain organoids, and that dual SMADi and SAG were not directly related to brain organoid caudalization events.

Figure 4.6B compared the four caudal groups with the group cultured under original Andersen's protocol (caudal original) regarding to the expression of the posterior genes along the neural tube. This result suggested that "Dual SMADi + SAG ca" organoids had the highest expressions for all three genes. Combining this with the immunostaining results, the "Dual SMADi + SAG ca/ro" protocols were chosen to proceed with elongated brain organoid differentiation and microfluidic gradient exposure experiments.

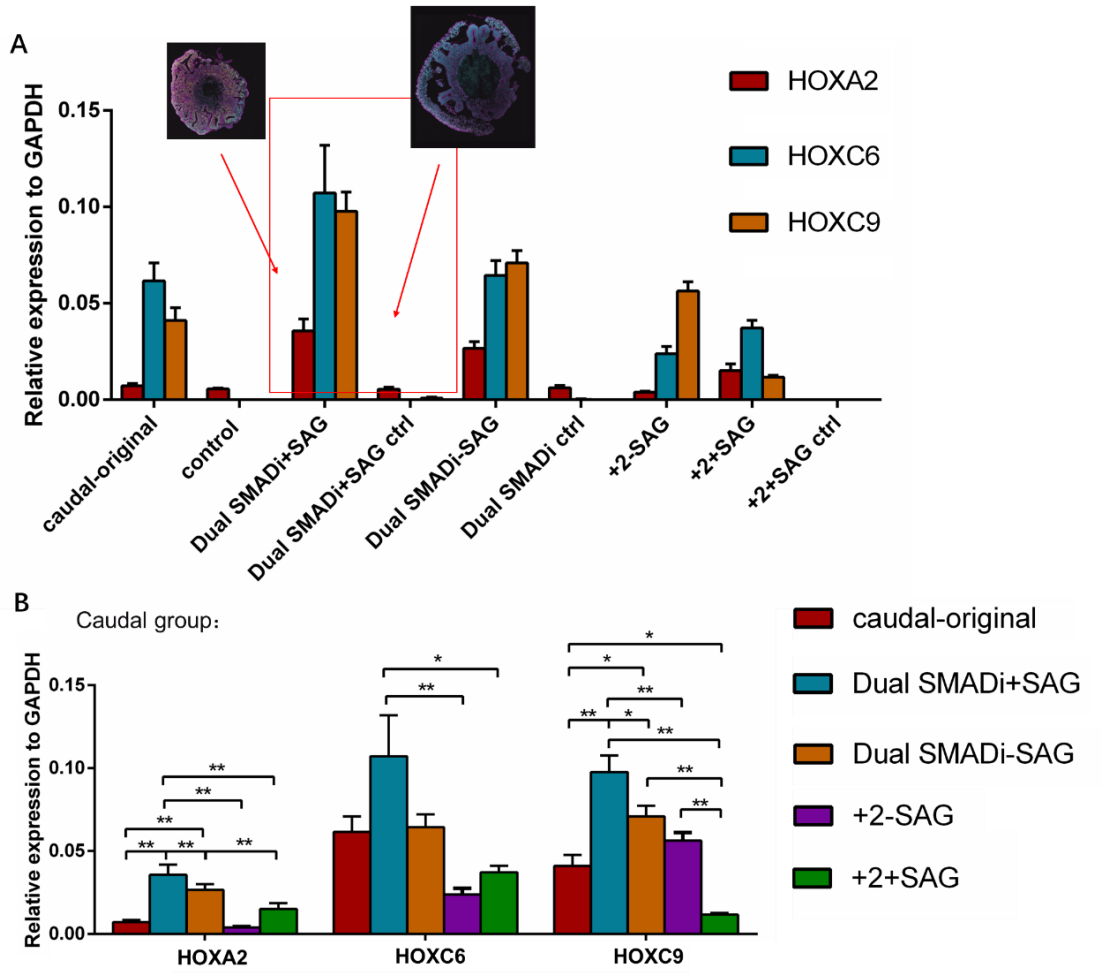


Figure 4. 6. A) q-RT PCR result for all groups. N = 4. **B)** qRT-PCR and statistical analysis results for the caudalized organoids, using one-way ANOVA and Sidak's test for each gene separately. $P < 0.05$, N = 4. *HOXA2* expresses in the hindbrain area; *HOXC6* expresses in the brachial area; *HOXC9* expresses in the thoracic area.

4.3.2 Long-term culture

To obtain more mature brain organoids for deeper investigation on signaling pathways and electrophysiology experiments, a 40-day organoid polarization protocol should also be prepared. Following Andersen's long-term culture protocol (Figure 4.7A[41]) and the microfluidic optimization plan that was decided in section 4.2.1 (Figure 4.7B), after day 20, the effect of growth factors (IGF-1, BDNF, AA, cAMP) and DAPT (notch pathway modulator) were studied. The experimental groups were listed in Figure 4.7C, with "9dm" referring to the 9-day microfluidic patterning plan (Fig 4.7B), "+fa" referring to the addition of all factors including DAPT from day 20 to day 24, IGF-1, BDNF, AA, cAMP from day 20 to day 40; "- DAPT" referring to the addition of IGF-1, BDNF, AA, cAMP from day 20 to day 40; "ca" and "ro" referring to the caudal group

and rostral group respectively.

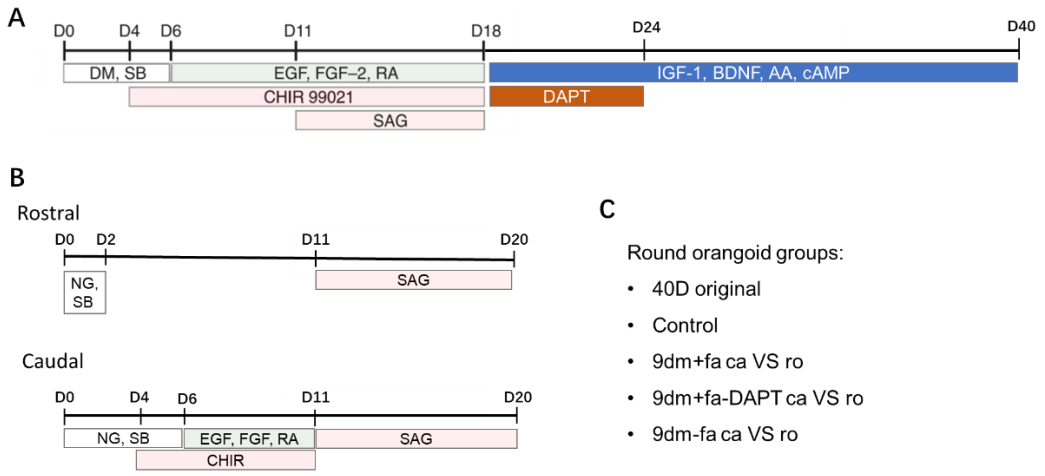


Figure 4. 7. A) Andersen's 40-day caudalization protocol[41]. **B)** The determined 9-day microfluidic patterning plan for 20-day organoid culture. **C)** The experimental groups included in this part of comparison.

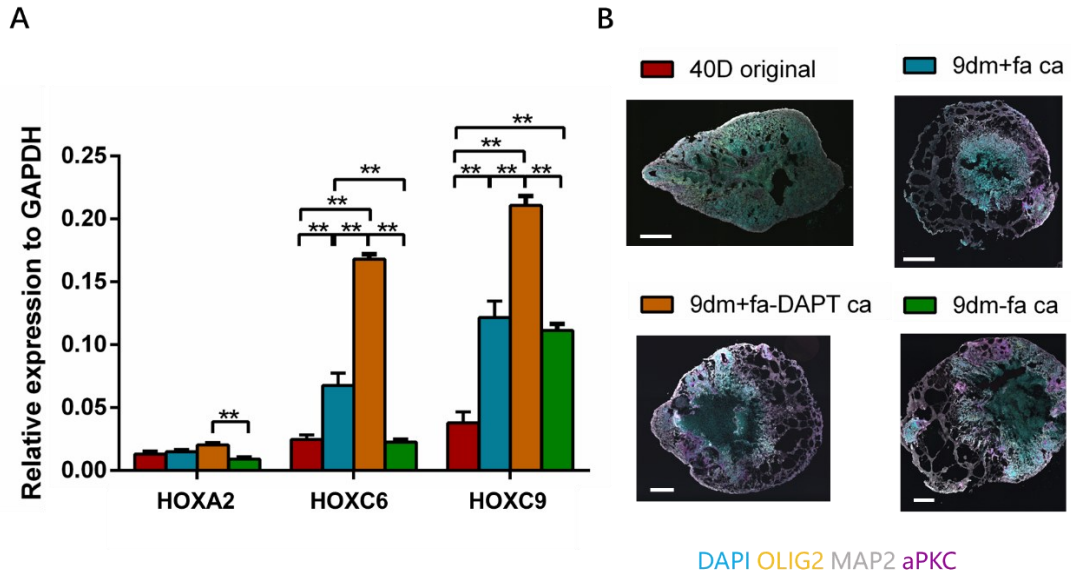


Figure 4. 8. A) q-RT PCR result for caudal groups. One-way ANOVA and Sidak's test was used to compare the group means with each other, for each gene separately. $P < 0.05$. $N = 4$. **B)** The confocal images were merged with DAPI (cyan), OLIG2 (Yellow), MAP2 (grey) and apical protein kinase C (aPKCζ) (magenta). Scale bars = 500 μm.

The qRT-PCR results for the caudal groups (Figure 4.8A) indicated that "9dm+fa-DAPT ca" organoids had the highest caudal brain marker expression. Moreover, the rostral groups had low to no caudal identity expression in all cases (Figure S3). However, the morphologies of the organoids cultured by the three modified protocols

were poor compared to the group cultured under the original 40-day protocol (Figure 4.8B), where the classic lumen budding structures were compromised. This issue will require more replications and investigation. Future studies shall focus on the “9dm+fa-DAPT ca” group and its rostral pair.

4.4 Material screening

4.4.1 Scaffold materials

As mentioned in section 1.7, silk, PCL, and PDO suture threads were chosen in the first place as scaffold materials for guiding brain organoids growth. However, the commercial silk suture threads with a diameter of 600 μm were too thick (Figure 4.9A and B) that hESCs failed completely to attach to the scaffolds in preliminary experiments. The degummed silk fibers were used instead (Figure 4.9C), as the effect of SF on brain organoid growth was still worth investigating. On the other hand, the size of micro-scaled silk fiber was closer to the traditional scaffold materials used in brain organoid studies, which could provide a suitable reference when discussing the effect of scaffold sizes on brain organoid growth.

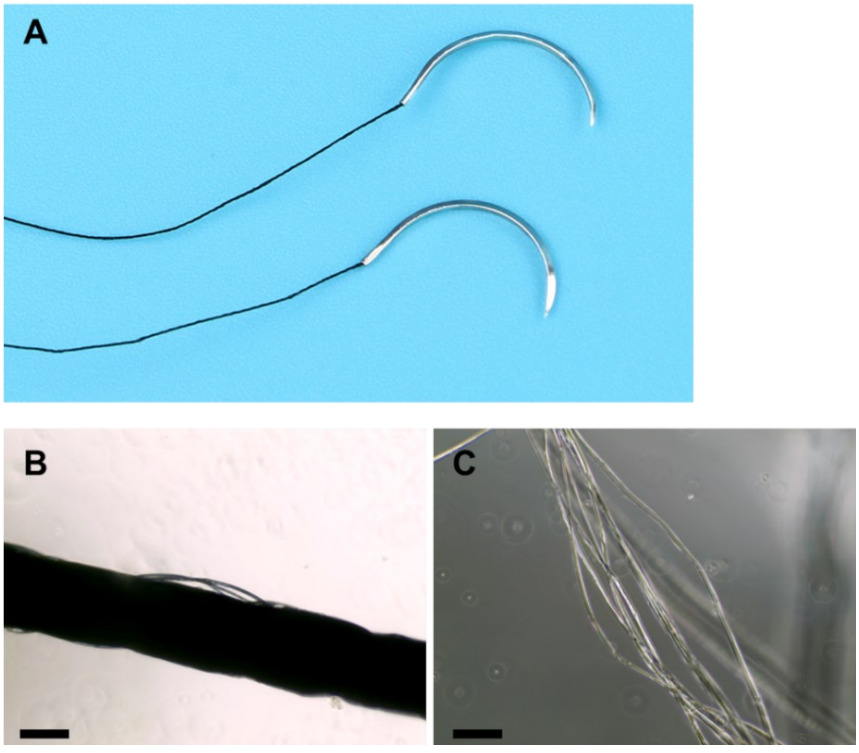


Figure 4. 9. A) Photo of commercial silk suture thread with needles. **B**) BF image of silk suture thread, with fibers bundled together. **C**) BF image of degreased silk fibers. Scale bars = 500 μm.

The commercial face-lifting threads circulating on the marked were selected as follow: 20G PCL, 20G and 27G PDO. The 20G PCL and PDO suture threads had similar diameters to the silk suture threads (Figure 4.10 A, B, D, and E), but with smooth surfaces that allowed hESCs to attach and grow. The 27G PDO was much smaller with an approximate diameter of 240 μm (Figure 4.10 C, and F), which provides an intermediate scale between 600 μm suture thread and micro-scaled fibers.

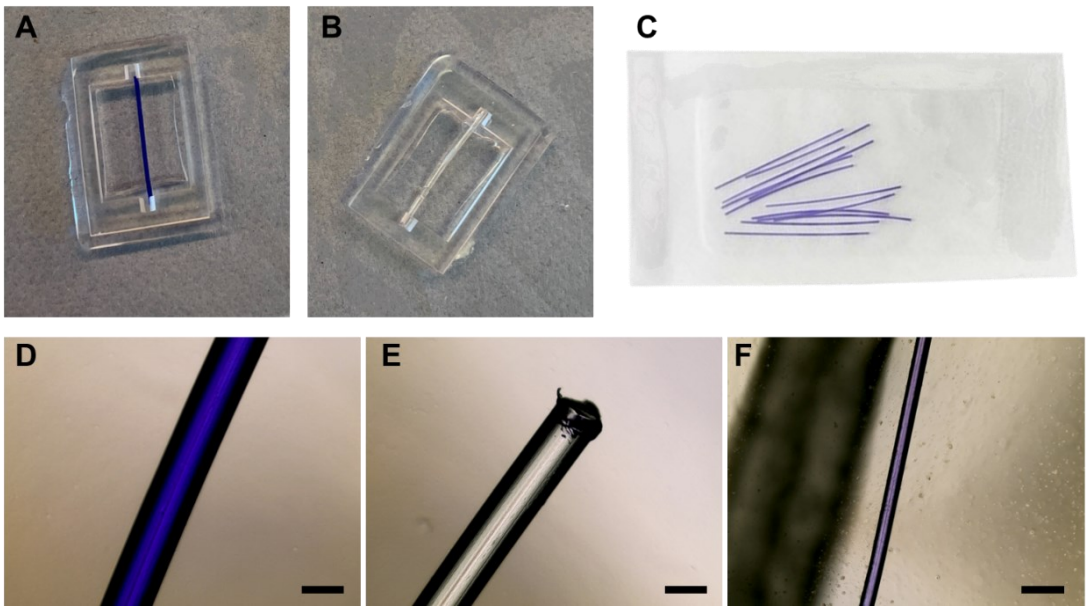


Figure 4. 10. Photos of commercial 20G **A)** PDO and **B)** PCL suture threads on PDMS holders. **C)** Photo of commercial 27G PCL suture threads in package. **D)** BF image of 20G PDO suture thread. **E)** BF image of 20G PCL suture thread with the edge caused by scissors cut. **F)** BF image of 27G PDO suture thread with the shadow of cell crown. Scale bars = 500 μm.

4.4.2 Brain organoid viability test

Following section 3.3.1, organoids grown on the fractures of the selected materials were captured with BF microscopy (Figure 4.11A). The results showed that single silk fiber barely supported cell attachment and organoid formation, and multiple silk fragments led to cell spontaneous differentiation. The immunostaining with SOX2, MAP2, and aPKCζ (Figure 4.11B) further confirmed that silk fibers failed to support brain organoids formation. On the other hand, both the PCL and PDO suture threads succeeded in supporting brain organoids formation. On day 20, the expansion of neuroepithelium buds was observed evenly around the material. With a diameter of 600 μm, 20G PCL and PDO largely expanded the material surface area for cell attachment, thus ensuring enhanced nutrient exchange efficiency.

Unlike traditional round organoids, there was no necrosis core area observed in the

PDO/PCL-guided organoids, which indicated a better cell viability that potentially supported longer term brain organoid maturation and the subsequent studies. In addition, a thinner 27G PDO scaffold with a diameter of 240 μm was also tested (Figure 4.11A). The neuroepithelium buddings were also observed around the scaffold without necrosis core area. Such a smaller size is closer to the traditional tissue engineering scaffold and suggests the possibility of illustrating the size effect on organoid generation.

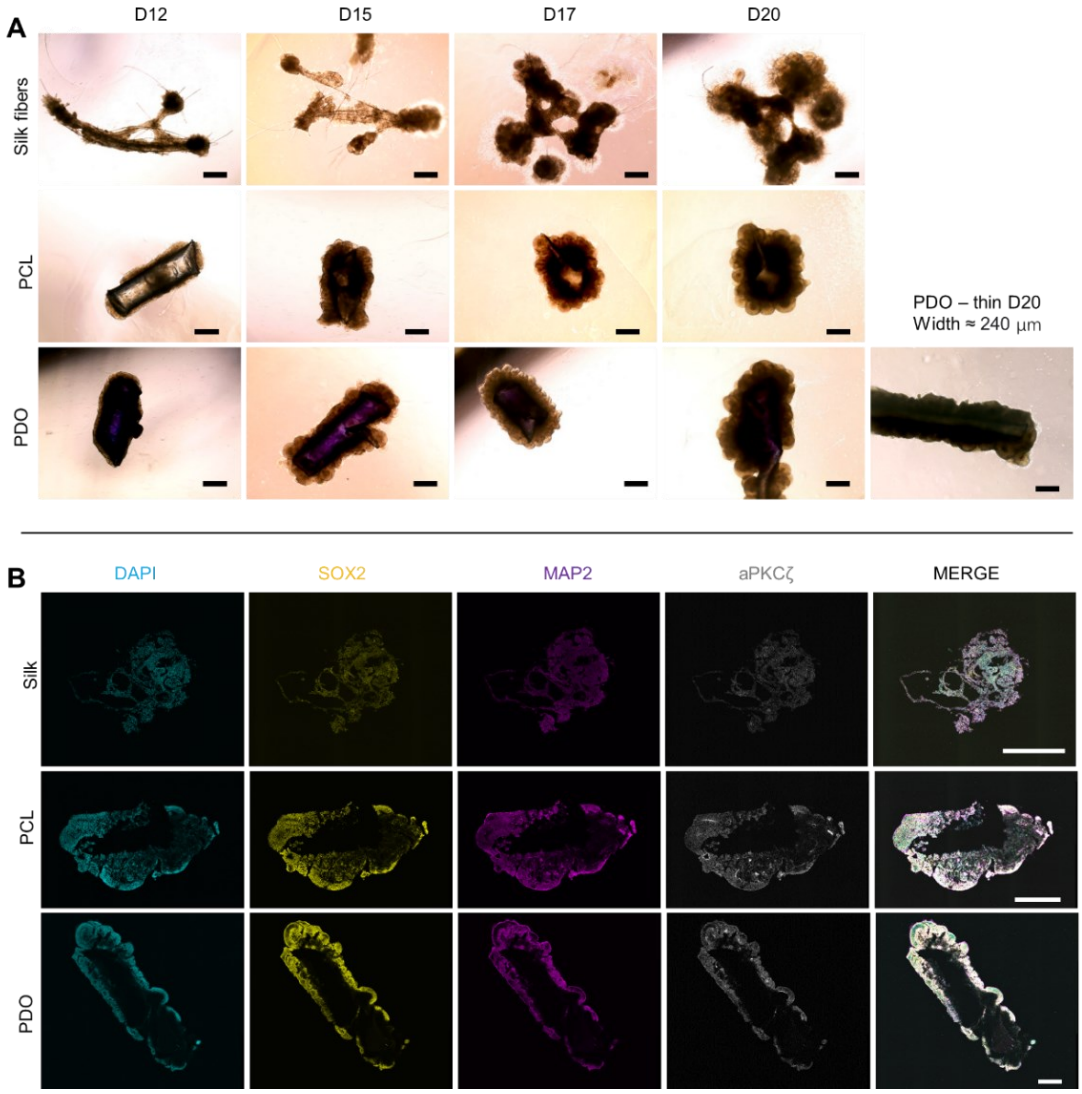


Figure 4. 11. A) BF images for 96 well plate material screening. **B**) Immunostaining and confocal microscopy images for day 20 organoids induced by different material fractures. Scale bars = 500 μm.

4.5 Anteroposterior patterning with microfluidic platform

4.5.1 Elongated organoid preliminary experiments

PDO and PCL scaffolds were further tested to generate elongated brain organoids. Although PCL worked well in the small fragment format, the 2 cm scaffold could hardly support stable organoid attachment. The organoid easily detached from the PCL scaffolds on day 17 orbital shaking (Figure S4). Brain organoids on 2 cm PDO, however, remained firmly attached during the entire culture period and thus were suitable for the microfluidic patterning experiments and further analysis. Therefore, the 20G and 27G PDO were decided as scaffold materials for elongated brain organoid culture.

The rostral and caudal protocol for short-term culture, determined in section 4.2.1, were then performed to induce brain organoids on both 27G (Figure 4.12) and 20G (Figure 4.13) PDO suture threads. The BF results showed that the organoid morphologies on PDO suture threads were consistent with the round organoids respectively, as the caudalized organoids were looser than the rostral ones, and the rostral organoids was surrounded by a thick layer of neurons.

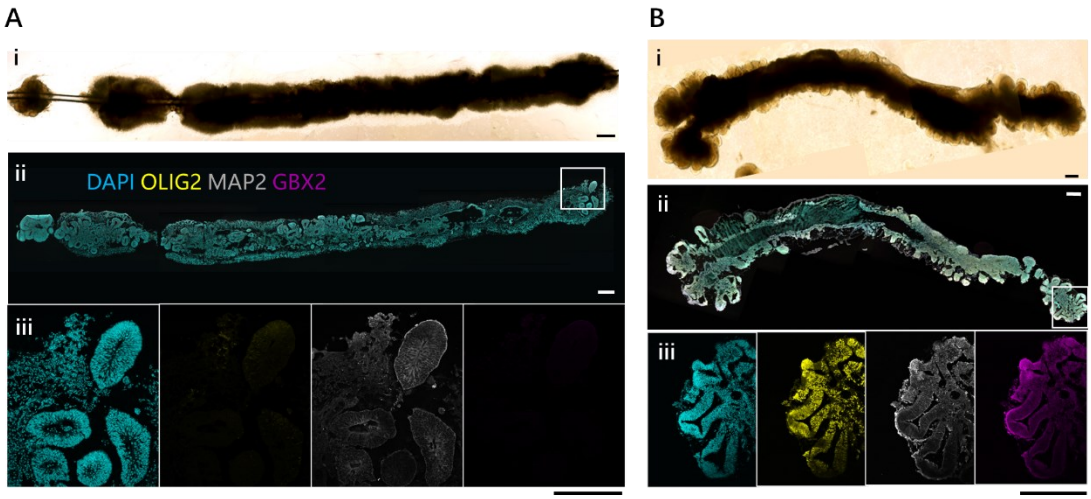


Figure 4. 12. 27G PDO-guided elongated organoid on day 20 under still condition with **A)** rostral and **B)** caudal differentiation protocol. The overall morphologies were observed with both **(i)** bright field and **(ii)** confocal microscopy, which merged four channels including DAPI (cyan), OLIG2 (yellow), MAP2 (grey) and GBX2 (magenta). Partial views under confocal microscopy **(iii)** zoomed up the white square area in **ii**, with all channels separated. Scale bars = 500 μm.

The motor neuron marker OLIG2 and hindbrain marker GBX2 were chosen to check the caudal identity for both organoids growing on 27G and 20G PDO scaffolds. The

immunostaining results (Figure 4.12 and Figure 4.13) showed that the caudal identity was only found in the caudal organoids but not in the rostral ones, suggesting that the patterning protocols were also effective in inducing elongated brain organoids differentiation, not interfered with by the supporting materials.

It is interesting to note that the 20G PDO scaffold-mediated organoids had a larger size than the 27G PDO scaffold-mediated organoids, possibly due to the larger surface area provided by the material. Besides, the 20G PDO scaffold-mediated rostral organoid showed more organized lumen budding than the 27G PDO scaffold-mediated one. Future studies could focus on a deeper analysis of gene expression to illustrate the influence of material size on organoid growth. Since the diameter of the scaffold used in previous papers[16, 76] for supporting organoid growth is closer to that of 27G, the following microfluidic patterning experiments started with 27G PDO scaffold in this stage. On the other hand, the 20G PDO scaffold could be used in the future with the cell crown modified accordingly.

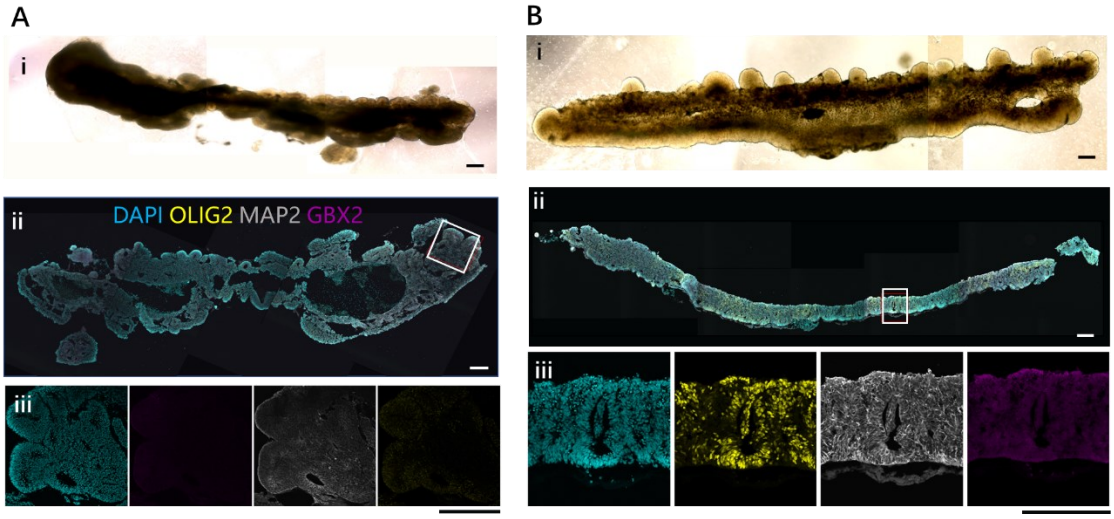


Figure 4. 13. 20G PDO-guided elongated organoid on day 20 under still condition with **A)** rostral and **B)** caudal differentiation protocol. The overall morphologies were observed with both **(i)** bright field and **(ii)** confocal microscopy, which merged all channels including DAPI (cyan), OLIG2 (yellow), MAP2 (grey) and GBX2 (magenta). Partial views under confocal microscopy **(iii)** zoomed up the white square area in **ii**, with all channels separated. Scale bars = 500 μm.

Before the microfluidic polarization experiment, the effect of microflow on organoid growth was also examined with 27G PDO-guided elongated brain organoids. The growth of organoids under static (Figure 4.14A) and microfluidic conditions (Figure 4.14B) without any morphogen supplement were compared as a group. Immunostaining results of the neural stem cell marker SOX2, neuron marker MAP2,

and the apical marker aPKCζ demonstrated the appearance of ventricular zone-like lumens in both organoids. This result suggested that microfluidic shear stress did not affect organoid growth so brain organoid elongation was achieved with all the classic brain organoid features maintained. However, the microfluidic-organoid (Figure 4.14B) tended to detach from the scaffold during the MG embedding process. Optimizations on the MG embedding should be performed to prevent the organoid from detaching and facilitate stable elongated organoid morphologies.

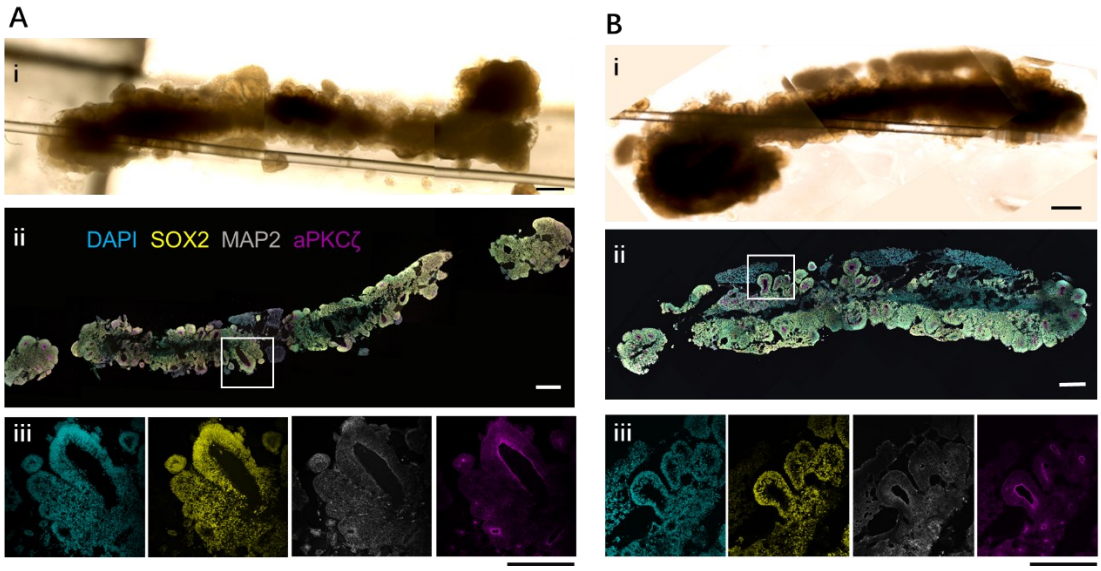


Figure 4. 14. 27G PDO-guided elongated brain organoid on day 20, cultured without any morphogens under **A)** still and **B)** microfluidic conditions. The overall morphologies were observed with both **(i)** bright field and **(ii)** confocal microscopy that merged all channels including DAPI (cyan), SOX2 (yellow), MAP2 (grey) and aPCKζ (magenta). Partial views under confocal microscopy **(iii)** zoomed up the white square area in **ii**, with all channels separated. Scale bars = 500 μm.

4.5.2 Anteroposterior patterning with microfluidic platform

As described in section 3.4, triplicate experiments were performed with 27G PDO-guided elongated brain organoids. After microfluidic patterning with the plan determined in 4.2.1, however, the organoid structure turned loose and fragile, so they broke off into small fragments on day 11 when terminating the microfluidic device and trying to lift the organoid-scaffold-cell crown assembly out of the culture chamber (Figure 4.15).

Forebrain marker FOXG1, floor plate marker FOXA2, caudal brain maker GBX2, and motor neuron marker OLIG2 were stained with three cryo-sectioned slices separately. Results (Figure 4.15) showed no caudal or rostral identity, but the floor plate marker was observed all over the fragments. Perhaps in the microfluidic chamber,

the morphogen gradients were interfered with air bubbles and mixed up homogeneously and made a 50% concentration that generated identity in the middle of the anteroposterior axis. In the future, comparative experiments should be conducted on round organoids with 50% morphogen concentration to verify a such hypothesis. Further optimizations on experimental handling should make sure a consistent and stable gradient in the microfluidic chamber and keep the organoid whole.

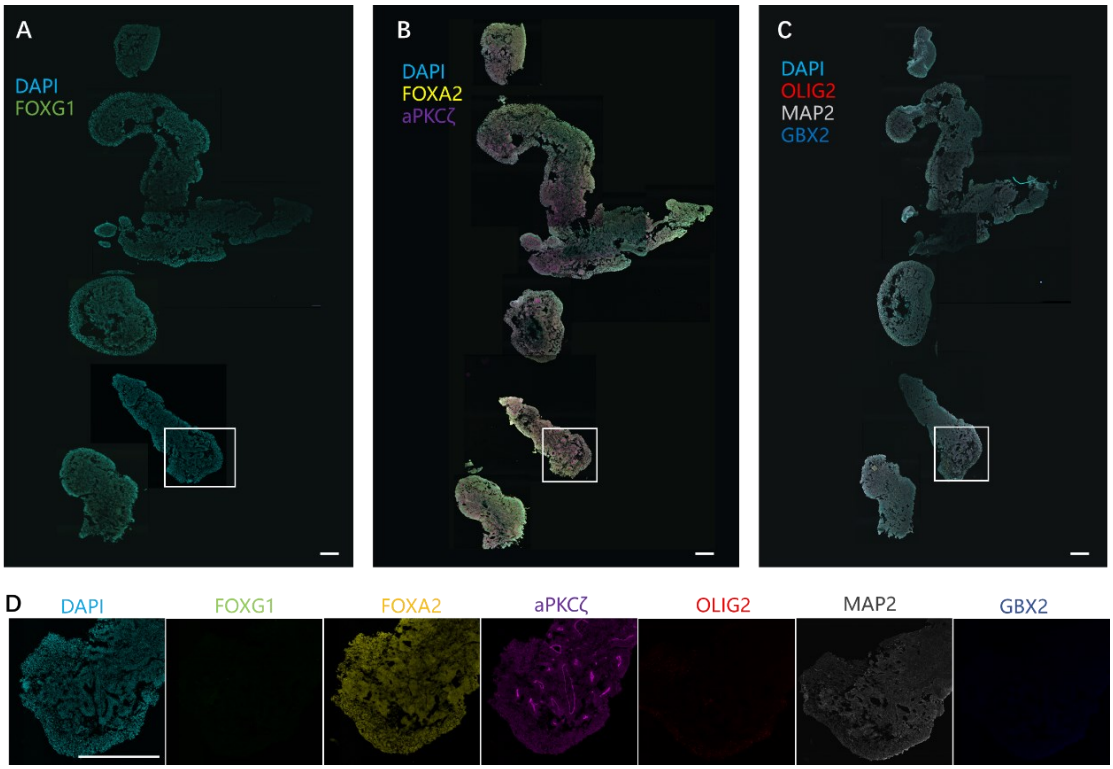


Figure 4. 15. The overall views for the fractured organoids aligned by the corresponding positions as they were on the scaffold. All channels were merged, stained with: **A)** DAPI (cyan) and FOXG1 (green); **B)** DAPI (cyan), FOXA2 (yellow) and aPKCζ (magenta); **C)** DAPI (cyan), OLIG2 (red), MAP2 (grey), and GBX2 (blue). Scale bars = 1 mm. The partial view **D)** separated all channels and zoomed up the white square areas in **A)**, **B)**, and **C)**. Scale bars = 500 μm.

5 Discussion

5.1 Microfluidic based brain organoid polarization platform

The microfluidic sequential mixer with serpentine channels was first brought up by Jeon et al. in 2000, explaining a simple, highly adaptable methodology to generate gradients with different shapes, types, and kinds (static and dynamic) through customized CAD design[95]. However, there were a lot of serpentine bending angles in the micro-scaled channels, it was very easy to generate bubbles and disturb microflows. Despite various optimization attempts in the presented study, including slowing down the flow rate gradually, using pumps with precise control, and prewarming the syringes and media, microbubbles remained a significant issue that would often cause failure in gradient generation.

Figure 4.2 proved a linear concentration gradient in the microfluidic chamber, but the brain organoid anteroposterior patterning plan was still unsuccessful, according to section 4.5.2. It was possible that the existence of a cell crown-scaffold-organoid set in the culture chamber disturbed gradient formation. And during microfluidic chip assembly, in order to guarantee the viability of the brain organoid, operation time should be reduced to minimal, which might cause leakage or loosening in the microfluidic chip.

Besides optimizing the chip design and practice the assembly process, an improvement on the microfluidic chip quality is also in demand. The formation of air bubbles was likely due to temperature differences, soluble gases, and the roughness of the microfluidic channels. The 3D printing machine that was used in this project had a 25 μm resolution, and the micro-channel width was 200 μm. Therefore, such 3D printer might leave a coarse surface on the mold that graved on the PDMS chip (Figure S5). In Kirkeby's paper[70], however, the negative mold was fabricated with plastic polyoxymethylene by micro-milling. And they used a thin layer of PDMS bottom instead of sealing with glass directly to reduce the shear stress caused by material differences[96]. These strategies are reliable to be applied in future work to prevent air bubble formation and optimize the fabrication of the microfluidic chip.

On the other hand, in section 4.4.1 ~ 4.4.2, both 27G and 20G PDO suture threads were examined as biocompatible materials for brain organoids elongation and morphogen-induced differentiation. However, for our microfluidic chip design (Figure

3.1A), the 4 mm chamber height was determined by the thickness of the cell crown fixing scaffold with lower hardness and strength, like 27G PDO thread and silk fiber. Such cell crown does not fit with the 20G PDO thread, which can be directly put on both edges of the chamber and support itself like a bridge. With a simple positioner to prevent the scaffold from moving, the depth of the culture chamber can be reduced accordingly. Based on the previous experiments on 2 mm-chamber chips (Figure 4.1B), we assume such gradient will be more stable than the 4 mm-chip designs. Future investigations on 20G PDO scaffold and its optimized microfluidic chip can be performed to verify the influence of height difference on maintaining a stable chamber gradient.

In general, the establishment of the microfluidic brain organoid patterning platform for *in vitro* brain organoid polarization was partially finished. It was an unprecedented trial exploring the combination of microfluidic gradient generator with scaffold-mediated brain organoid. Such a platform held flexibility and controllability, enabling various modifications based on material or different patterning protocols, and was worthy of deeper exploration.

5.2. Morphogen regulations for 20-day brain organoid anteroposterior patterning

The formation of EB is a process of 3D organization that resembles the initial segregation of extraembryonic and embryonic tissues, including trophectoderm, primitive endoderm, and early mesoderm[97]. Such cell differentiation and spatial sorting are fundamental for the formation of an epithelia-like cell sheet on the EB surface, which is also the basic event for the generation of neuroectoderm in the subsequent neuronal induction. Section 4.3.1 compared the effect of dual SMADi and SAG on rostral/caudal differentiation of the organoids, focusing on their different combinations and timings of supplement. For the caudalized organoids, “+2 +/- SAG ca” referred to the Dual SMADi treatment started on day 2 instead of day 0, as explained in Figure 4.4, leading to a result with caudal identity remained (Figure 4.6, S1), while the organoid morphologies were deteriorated (Figure 4.5, S1). However, the caudal organoids with Dual SMADi from day 0 (Dual SMADi +/- SAG ca) managed to maintain organoid morphologies. These results indicated that the timing of Dual SMADi treatment is crucial, which must start before the formation of the epithelia-like cell sheet on the EB.

SMAD proteins are a group of signal transmission proteins that play an essential role in BMP and TGF-β pathways, which are involved not only in neural induction but also in bone development and cancer progression[98, 99]. Dual SMAD inhibition that includes the use of Noggin and SB431542 is a methodology that specifically blocks SMAD signaling via inhibiting the TGFβ and BMP pathways in an EB-based protocol, which rapidly induces hESCs to differentiate into early neuroectoderm[93].

The determined caudalization protocol mainly relies on the Wnt signal activation with CHIR, which also has many other roles in early embryogenesis, such as dorsalization and mesoderm tissue generation[100]. Therefore, the use of dual SMADi is a prerequisite condition for Wnt signal to establish robust and lasting brain organoid caudal identity, preventing the ESCs from differentiating towards mesodermal fate[101]. Immunostaining (Figure 4.5, S1) and qRT-PCR results (Figure 4.6) have demonstrated the success of brain organoid caudalization using Dual SMADi and CHIR, that activates Wnt signal. However, for the rostral groups without Wnt signal activation, dual SMADi treatment in the first two days led to an abnormal morphology with layers of neurons surrounding it (Figure 4.5, S1, Dual SMADi - SAG ro).

To our understanding, for monolayer cell culture, dual SMADi induces neural rosettes formation and generates different types of neurons[102], which is not ideal for brain organoid-generating protocol. With TGFβ and BMP pathway blocked by Noggin and SB431542 in the first two days, the subsequent neural induction and the formation of neural ectoderm tissue were interfered, resulting in an abnormal morphology of the “Dual SMADi - SAG ro” organoid (Figure 4.5, S1). However, the addition of SAG after day 11 (Dual SMADi + SAG ro) has improved such situation by maintaining organoid morphology, as shown in Figure 4.5 and Figure S1. Similar findings of SAG facilitating brain organoid morphology were also found in the caudal groups, comparing the “Dual SMADi +/- SAG ca” organoids (Figure 4.5, S1). qRT-PCR results further proved the upgrading of caudal gene expression with the presence of SAG (Figure 4.6). The motor neuron marker OLIG2 expression was also observed in the “Dual SMADi + SAG ca” organoid (Figure 4.5, S1), which was even better than the original Andersen’s protocol generated brain organoid (Figure S2). These results indicated that SAG might have crosstalk with dual SMADi treatment. A possible examination target could be the BMP pathway that both SAG and dual SMADi are linked with[103, 104]. A ligand binding assay could be used to verify this assumption, which is a very interesting point to investigate in the future.

In addition, SAG has been used as an SHH signal agonist that combines with IWP2 generating a ventral identity for brain organoids. Literatures also suggested that a low

concentration of SAG would augment the proliferation and the survival of neural cells[105]. In the rostral groups tested in 4.2.1, for the one with only SAG supplement after day 11 (+2 + SAG ro), the organoids formed membrane-like structures folding around the core, which was likely to be ventricular-like structures cuddling together (Figure S1, Figure 4.4). Such morphology was very usual, only similar to the choroid plexus organoid reported in 2020, which was patterned from EB exposed to BMP and CHIR that activate Wnt signals[106]. In the future, comprehensive immunostaining is required, including the choroid plexus epithelium marker TTR[107, 108], to identify the cell types within the membrane-like structures and promote the understanding of the effect of SAG on brain organoid polarization.

Moreover, the comparison between Dual SMADi + SAG ca protocol and the original Andersen's protocol (Figure 4.6, S2) provided insights into brain organoid caudalization. The only difference is the timing of the addition of CHIR, EGF, FGF, and RA, which are very effective caudalizing factors, as previous described[109]. In Andersen's protocol, these factors were supplemented from day 4 to day 20, while in the "Dual SMADi + SAG ca" protocol, the addition of these factors was terminated on day 11 before MG embedding and SAG supplement. In this case, the interaction between the Wnt signal and SAG was excluded. To note, Wnt is also involved in neural tube dorsalization, while the SHH signaling pathway that SAG agonized induces ventral polarization. Therefore, the effect of CHIR (Wnt activator) and SAG might be inhibited by each other. For the "Dual SMADi + SAG ca" organoids, after MG embedding, when large buds of continuous neuroepithelium were formed, the supplement of SAG could modulate early spontaneous electrical activity in the embryonic spinal cord, which is crucial for spinal neuron differentiation and GABAergic phenotype homeostatic specification[110]. This might be an explanation for the OLIG2 expression and upgraded *HOXC6, HOXC9* gene expressions. These results facilitated our understanding on generating spinal cord organoids and the studies about SAG – Wnt signal crosstalk. A deeper illustration shall require RNA seq to map the cell differentiation events and reveal the brain anteroposterior mechanisms at a genetic level.

Regarding the second aim in section 2, results in section 4.3.1 achieved an optimal rostral/caudal patterning protocol for short-term microfluidic culture. Multiple combinations of drug treatment and the influence of timing on brain organoid caudalization were discussed, emphasized the significance of brain organoids as *in vitro* brain model to illustrate neural induction, as previously, the biomolecular studies were performed with model animals.

5.3 Long-term culture

Section 4.3.2 explored the rostral and caudal protocols for 40-day brain organoid culture that can be applied in the determined 9-day microfluidic exposure plan (Figure 4.7B). Among the four caudal conditions including the original Andersen's protocol, "9dm+fa-DAPT ca" exhibited the highest expressing level of *HOXC6* and *HOXC9*, indicating that with the modification from day 2 to day 20, the notch pathway modulation of DAPT[111] was not necessary anymore. On the other hand, the morphologies of brain organoids under modified caudal conditions ("9dm+fa ca", "9dm+fa-DAPT ca", "9dm-fa ca") were deteriorated, and surprisingly, the expression of OLIG2 was also lost (Figure 4.8B). Since the morphologies of the original Andersen's protocol-induced organoids were maintained, it was indicated that our modifications (Dual SMADi + SAG ca/ro) on the Andersen's protocol were incompatible with the cultivation plan from day 20 to day 40.

20-day brain organoid only generates rudimentary neuroepithelia structures that are composed of neural progenitor cells. For organoids cultured beyond 40 days, however, more specific neuron cells could be observed, leading to an identical layer of cell sorting, as shown in Figure 1.2D. In this stage, functional studies can be conducted, such as neuron migration, calcium imaging, and electrophysiology[40, 42]. Additionally, mechanism studies for long-term cultured brain organoids have significant importance in interrogating the complex genetic regulatory system and the concentration-dependent effect of natural brain regionalization.

Therefore, the aim to generate mature polarized brain organoid has not been achieved yet. To better evaluate the presented microfluidics-based platform, an applicable 40-day microfluidic patterning protocol is required in the future, maintaining the basic epithelial morphology of brain organoids. More comprehensive experiments with different factors and exposure periods are expected with round organoids.

Single-cell transcriptomics and spatial transcriptomics are powerful tools that can be used to study the trajectory of anteroposterior polarization in the engineered brain organoids[112]. These techniques allow for global profiling of the gene expression of large populations of individual cells[113]. In the future, brain organoids at different stages/positions can be harvested during the polarization process and then perform transcriptomic analysis to determine the spatial and temporal changes in cell phenotype, including the expression of genes related to stemness, neural differentiation, and polarization. Once the long-term culture protocol is determined, the

development of the engineering neural tube can be mapped to examine the differences between 20-day and 40-day organoids. This will provide a better understanding on the developmental trajectory of the polarized organoids, providing a versatile platform for subsequent mechanism studies.

5.4 Elongated brain organoid generation

Before the material screening, the preliminary experiments discussed whether MG coating was essential for cell attachment (Figure S6). For silk fibers, the coating was effective to a certain extent but could not guarantee linear growth of brain organoids along the scaffolds. In fact, the cell attachment majorly relied on the cell amount surrounding the surface of the material. With MG coating, the same cell seeding density ($1.2 * 10^5$/mL) worked well with 96 well plate for material fragment seeding (Figure 4.8) but failed in 2 mm stretched material seeding for all kinds of materials. Because the U-bottom of 96 well plate aggregated ESCs while the 6 well plate suspended cells, which led to a considerably lower cells density around the material surface specifically. The seeding density in 6 well plate once was increased to $4.8 * 10^5$/mL for all materials (silk, PDO, and PCL), but results showed poor organoid attachment still. Such cell clusters either fell off the scaffolds or grew into spheres after day 11 MG embedding (Figure S7).

hESCs in suspension tended to gather and form small spheroids. 2 cm 20G PDO/PCL suture thread, like a stick, had a bigger surface area for such spheroids to settle and connect. The cell seeding with $4.8 * 10^5$/mL density succeeded in 4 ibidi well, where much smaller space than 6 well plate regulated all cell clusters and facilitated cell attachment. Once the cell clusters became a continuous layer that covered around the 20G PDO/PCL surface, cells survived and started to grow as a whole. 27G PDO was more like a fiber, so that a cell crown was necessary to fix it, and the surface area was comparatively small for hESC clusters to settle. Figure 3.2 shows how an agarose base was applied to make a groove that fixed both the cell crown and the scaffold, and significantly increased cell density to $2*10^7$/mL.

This way, cell clusters did not settle on the material surface, and the organoid morphology was not guided by the material. It was the groove that regulated hESC clusters to form an elongated EB that buried the scaffold inside. When removing the cell crown-scaffold assembly on day 2, the elongated EB was passively carried out with the 27G PDO, then grew along with it. Such seeding methodology provided a new idea about regulating the shape of brain organoids via a narrow groove structure rather

than scaffold materials. It was based on the fact that EB is composed of an epithelia-like cell sheet on the surface, which is mediated by the cell-cell adhesion that supports self-organization[97]. In this case, EBs with more flexible shapes and connected types can be produced in the future, for example, a bridge or even a net-like structure.

Figure 4.9 shows the way neuroepithelium grew on fracture of materials including 20G PDO, 27G PDO, and 20G PCL, where the necrotic core of traditional round organoids that limited their size seemed invisible. This observation suggested that the efficiency of neuroectoderm formation was significantly improved via scaffold guidance, which coincided with Lancaster's previously described[76]. However, whether such improvement has been linked to the size of the supporting scaffold remains unknown. Figure 4.10B. i, ii, Figure 4.12A. i, ii, B. i, ii showed the brain organoids elongated via 27G PDO with different culture protocols. A hollow area was observed within all the organoids above, making a tube-like structure of the brain organoids. It was hard to determine whether the hollow area was caused by the 27G PDO or also caused by inner necrosis. Cell viability, the efficiency of oxygen, and nutrient exchange should be examined in the future to provide evidence for material screening that further optimizes the whole microfluidic brain organoid patterning platform.

To sum up, the hypothesis that commercial suture threads could be used as scaffold materials regulating the shape of brain organoids has been perfectly proved, thus providing an alternative strategy in generating tissue engineering. The major considerations focused on the tensile strength, surface properties (smooth or rough) and the accessibility on the market. However, the commercially processed suture threads might hinder the natural chemical properties. Therefore, the exploration in this project on material-brain organoid interaction remained relevantly superficial and left significant advancing space for studies in the future.

6. Future work

First of all, optimizations on microfluidic chip fabrication should be performed to reduce the appearance of air bubbles, and improvement on day 11 MG embedding should be done to prevent the organoid from breaking off after microfluidic patterning stimuli. Afterwards, replication of the 20-day anteroposterior microfluidic brain organoid patterning experiment can be conducted to verify the application of such microfluidics-based platform in guiding brain organoid polarization. Secondly, exploring the 20G PDO as an alternative material to provide flexibility to the microfluidic brain organoid patterning platform. Thirdly, the 40-day organoid patterning protocol should be determined via round organoid screening.

The effect of morphogen gradient in development is very complicated and essential. Naturally, the gradients of Wnt, RA, and FGF are not working together in the same direction (Figure 6.1A)[114]. Therefore, packing all the caudalization factors together in the same media may not be ideal. Figure 6.1B shows an idea of using multiple microfluidic gradients to recapitulate the natural morphogen gradients in the anteroposterior axis more accurately. This approach would involve a Wnt gradient in the forebrain and hindbrain segment, and an opposing gradient of RA, FGF, and GDF11 in the spinal cord segment. Future advances can be achieved based on the flexibility of microfluidic design to make versatile gradients that induce more mature polarized brain organoids.

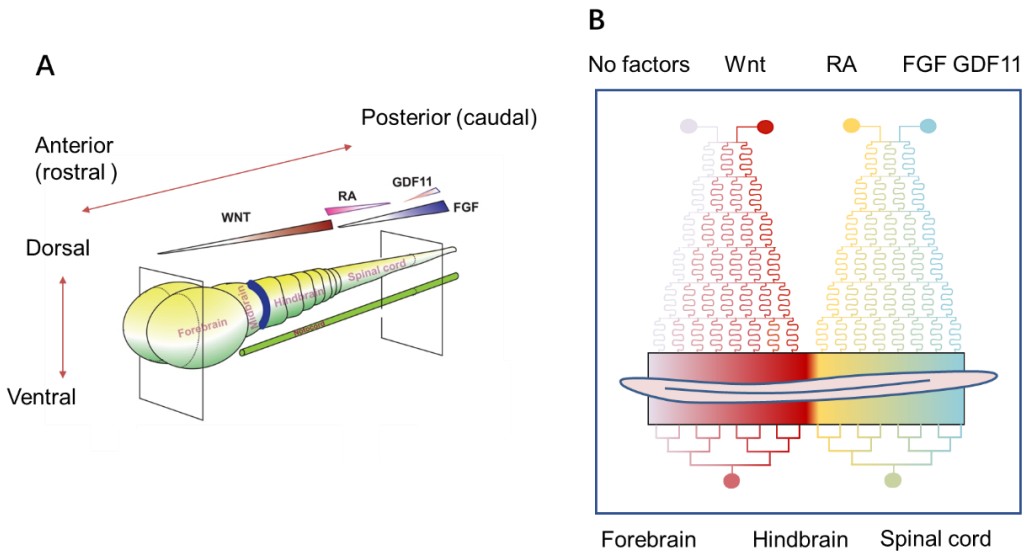


Figure 6. 1. A) The morphogen distribution along the anteroposterior axis of the natural brain. Adapted from Tao et al.[114] **B)** Schematics for multiple microfluidic gradients hypothesis.

7. Conclusion

This work has explored multiple morphogens in regulating brain organoids differentiation towards rostral and caudal fate, and different commercial suture threads in guiding brain organoid elongation, which are applicable for a novel microfluidics-based engineering platform for brain organoid anteroposterior patterning by providing a controllable morphogen concentration gradient.

The FSS indicator under a live cell microscope visualized the homogeneous mixing of two microflows in the microfluidic channels and a gradually increased gradient in the culture chamber, which was analyzed by ImageJ. The calculation of Pe and Re numbers suggested that the flow was dominated by laminar flow and advection in the culture chamber. However, air bubbles remained a significant issue that led to an unstable gradient damaging brain organoid anteroposterior polarization outcome. Further optimizations, such as increasing the printing resolution and using PDMS as a sealing bottom are expected to prevent microbubble formation.

Comparative experiments between different microfluidic chips revealed the fact that reducing the height difference between the microchannels and the culture chamber would facilitate a more stable chamber gradient, which provided insights into the design of such microfluidic gradient generator. With cell crown to fix thinner scaffold such as 27G PDO thread, 4 mm of chamber depth was required. However, a stronger scaffold such as 20G PDO thread can support itself and be fixed in the chamber with a simple positioner, thus largely reducing the height of the chamber. Such a strategy can be conducted in the future to expand the flexibility and application breadth of the presented microfluidic brain organoid patterning platform.

The effect of multiple morphogens included in neural tube anteroposterior patterning was explored via comparative experiments with round organoids. Dual SMADi supplement must start on day 0 before the formation of the epithelia-like cell sheet of the EB, otherwise the organoid morphologies would deteriorate. However, for the rostral groups, dual SMADi treatment in the first two days caused a thick layer of neurons surrounding the organoids, which might be related to the early neuronal inducement of dual SMADi before the cell sorting of EB happens. For both rostral and caudal organoids with dual SMADi treatment started on day 0, the addition of SAG facilitated organoid morphologies. Further examination shall focus on their common signal target, such as the BMP pathway, by a ligand binding assay and RNA-seq.

The “Dual SMADi + SAG ca” organoids exhibited the highest expression level of caudal neural tube genes *HOXC6* and *HOXC9*, and was the only condition generating motor neurons, with specific marker OLIG2 observed via immunostaining, which was even absent in organoids following the original Andersen’s caudalzaition protocol. The only difference between them was the exposure period of SAG and the caudalization factors (CHIR, EGF, FGF RA). The “Dual SMADi + SAG ca” protocol prevented the interaction between SAG and the caudalization factors, while the Andersen’s protocol used caudalization factors until day 20. Deeper illustration at the genetic level is required in the future to reveal the crosstalk between SAG and Wnt signaling pathways.

40-day long-term culture conditions were extended based on the “Dual SMADi + SAG ca/ro” plan, which was determined as the microfluidic anteroposterior patterning protocol for 20-day culture and 9-day microfluidic stimuli. However, all the caudal comparative groups failed to generate brain organoids with epithelial morphology and OLIG2 expression, despite the caudal gene expressions being maintained at a good level. Future experiments are required to find out a suitable plan for long-term culture, fulfilling the condition of organoid functional studies. “9dm+fa-DAPT” had the highest expression of *HOXC6* and *HOXC9* compared to the other 40-day caudal patterning groups, indicating that future optimizations can exclude notch pathway modulation.

Viability tests proved the biocompatibility of commercial suture threads (27/20G PDO and 20G PCL) in guiding brain organoid growth, while silk fibers failed to generate brain organoids in the 96 U-bottom well plate. MG coating of materials was necessary for hESCs attachment and EB formation, but silk fiber with a very small size also failed to support elongated brain organoid growth. In terms of the cell seeding with 2 cm suture threads, cell attachment also relied on high cell density of seeding. A 4 ibidi well with $4.8 * 10^5$/mL cell density succeeded with 20G suture threads (PDO/PCL) seeding. For the 27G PDO suture thread, an agarose groove structure was needed to aggregate hESCs maximumly and have the material buried into them.

The necrotic core of conventional round organoids was not observed in the 20G materials-guided brain organoids, which indicated an improved efficiency of neuroectoderm formation. Both 27G and 20G PDO suture threads succeeded in guiding elongated brain organoid growth and differentiation. Via immunostaining, differences in multiple markers expression were not found between them. But a hollow area was observed within the 27G PDO-guided brain organoids. More comprehensive staining and RNA-seq are expected to compare the difference in cell survival, differentiation trajectory, and cell-material interaction to reveal the effect of material size on brain organoid growth and differentiation.

Finally, the trial experiment on brain organoid microfluidic anteroposterior patterning pointed out the direction of further optimization. On the one hand, optimizations on microfluidic chip fabrication should be performed to provide a more stable chamber gradient. On the other hand, an improvement on day 11 MG embedding should be made to prevent the organoid from breaking off.

References

[1] Power J D, Cohen A L, Nelson S M, et al. Functional Network Organization of the Human Brain[J]. Neuron, 2011,72(4):665-678.

[2] Kelava I, Lancaster M A. Dishing out mini-brains: Current progress and future prospects in brain organoid research[J]. Dev Biol, 2016,420(2):199-209.

[3] Lancaster M A, Knoblich J A. Generation of cerebral organoids from human pluripotent stem cells[J]. Nature Protocols, 2014,9(10):2329-2340.

[4] Evans M. Discovering pluripotency: 30 years of mouse embryonic stem cells[J]. Nature Reviews Molecular Cell Biology, 2011,12(10):680-686.

[5] Nasu M, Takata N, Danjo T, et al. Robust formation and maintenance of continuous stratified cortical neuroepithelium by laminin-containing matrix in mouse ES cell culture[J]. PLoS One, 2012,7(12):e53024.

[6] Nasu M, Takata N, Danjo T, et al. Robust formation and maintenance of continuous stratified cortical neuroepithelium by laminin-containing matrix in mouse ES cell culture[J]. PLoS One, 2012,7(12):e53024.

[7] Lancaster M A, Knoblich J A. Organogenesis in a dish: modeling development and disease using organoid technologies[J]. Science, 2014,345(6194):1247125.

[8] Sidhaye J, Knoblich J A. Brain organoids: an ensemble of bioassays to investigate human neurodevelopment and disease[J]. Cell Death & Differentiation, 2021,28(1):52-67.

[9] Lancaster M A, Renner M, Martin C A, et al. Cerebral organoids model human brain development and microcephaly[J]. Nature, 2013,501(7467):373-379.

[10] Ying Q, Smith A G. Defined Conditions for Neural Commitment and Differentiation[M]//Methods in Enzymology. Academic Press, 2003:327-341.

[11] Denham M, Dottori M. Neural Differentiation of Induced Pluripotent Stem Cells[M]//MANFREDI G, KAWAMATA H. Neurodegeneration: Methods and Protocols. Totowa, NJ: Humana Press, 2011:99-110.

[12] Chiaradia I, Lancaster M A. Brain organoids for the study of human neurobiology at the interface of in vitro and in vivo[J]. Nature Neuroscience, 2020,23(12):1496-1508.

[13] Qian X, Nguyen H N, Song M M, et al. Brain-Region-Specific Organoids Using Mini-bioreactors for Modeling ZIKV Exposure[J]. Cell, 2016,165(5):1238-1254.

[14] Qian X, Song H, Ming G. Brain organoids: advances, applications and challenges[J]. Development, 2019,146(8).

[15] Camp J G, Badsha F, Florio M, et al. Human cerebral organoids recapitulate gene expression programs of fetal neocortex development[J]. Proceedings of the National Academy of Sciences, 2015,112(51):15672.

[16] Fiorenzano A, Sozzi E, Birtele M, et al. Single-cell transcriptomics captures features of human midbrain development and dopamine neuron diversity in brain organoids[J]. Nat Commun, 2021,12(1):7302.

[17] Rakic P. Evolution of the neocortex: a perspective from developmental biology[J]. Nature Reviews Neuroscience, 2009,10(10):724-735.

[18] Sousa A M M, Meyer K A, Santpere G, et al. Evolution of the Human Nervous System

Function, Structure, and Development[J]. Cell, 2017,170(2):226-247.

[19] Otani T, Marchetto M C, Gage F H, et al. 2D and 3D Stem Cell Models of Primate Cortical Development Identify Species-Specific Differences in Progenitor Behavior Contributing to Brain Size[J]. Cell Stem Cell, 2016,18(4):467-480.

[20] Lin Y, Seo J, Gao F, et al. APOE4 Causes Widespread Molecular and Cellular Alterations Associated with Alzheimer's Disease Phenotypes in Human iPSC-Derived Brain Cell Types[J]. Neuron, 2018,98(6):1141-1154.

[21] Cugola F R, Fernandes I R, Russo F B, et al. The Brazilian Zika virus strain causes birth defects in experimental models[J]. Nature, 2016,534(7606):267-271.

[22] Gabriel E, Ramani A, Karow U, et al. Recent Zika Virus Isolates Induce Premature Differentiation of Neural Progenitors in Human Brain Organoids[J]. Cell Stem Cell, 2017,20(3):397-406.

[23] Chen H I, Song H, Ming G. Applications of Human Brain Organoids to Clinical Problems[J]. Developmental Dynamics, 2019,248(1):53-64.

[24] Pham M T, Pollock K M, Rose M D, et al. Generation of human vascularized brain organoids[J]. Neuroreport, 2018,29(7):588-593.

[25] Takebe T, Enomura M, Yoshizawa E, et al. Vascularized and Complex Organ Buds from Diverse Tissues via Mesenchymal Cell-Driven Condensation[J]. Cell Stem Cell, 2015,16(5):556-565.

[26] Homan K A, Gupta N, Kroll K T, et al. Flow-enhanced vascularization and maturation of kidney organoids in vitro[J]. Nature Methods, 2019,16(3):255-262.

[27] Liu F, Huang J, Zhang L, et al. Advances in Cerebral Organoid Systems and their Application in Disease Modeling[J]. Neuroscience, 2019,399:28-38.

[28] Studer L, Vera E, Cornacchia D. Programming and Reprogramming Cellular Age in the Era of Induced Pluripotency[J]. Cell Stem Cell, 2015,16(6):591-600.

[29] Miura Y, Pașca S P. Polarizing brain organoids[J]. Nature Biotechnology, 2019,37(4):377-378.

[30] Kirkeby A, Grealish S, Wolf D A, et al. Generation of Regionally Specified Neural Progenitors and Functional Neurons from Human Embryonic Stem Cells under Defined Conditions[J]. Cell Reports, 2012,1(6):703-714.

[31] Koo B, Choi B, Park H, et al. Past, Present, and Future of Brain Organoid Technology[J]. Molecules and cells, 2019,42(9):617-627.

[32] Eiraku M, Watanabe K, Matsuo-Takasaki M, et al. Self-Organized Formation of Polarized Cortical Tissues from ESCs and Its Active Manipulation by Extrinsic Signals[J]. Cell Stem Cell, 2008,3(5):519-532.

[33] Pellegrini L, Bonfio C, Chadwick J, et al. Human CNS barrier-forming organoids with cerebrospinal fluid production[J]. Science, 2020,369(6500):z5626.

[34] Nakano T, Ando S, Takata N, et al. Self-Formation of Optic Cups and Storable Stratified Neural Retina from Human ESCs[J]. Cell Stem Cell, 2012,10(6):771-785.

[35] Jo J, Xiao Y, Sun A X, et al. Midbrain-like Organoids from Human Pluripotent Stem Cells Contain Functional Dopaminergic and Neuromelanin-Producing Neurons[J]. Cell Stem Cell, 2016,19(2):248-257.

[36] Muguruma K, Nishiyama A, Kawakami H, et al. Self-Organization of Polarized Cerebellar

Tissue in 3D Culture of Human Pluripotent Stem Cells[J]. Cell Reports, 2015,10(4):537-550.
[37] Ogura T, Sakaguchi H, Miyamoto S, et al. Three-dimensional induction of dorsal, intermediate and ventral spinal cord tissues from human pluripotent stem cells[J]. Development, 2018,145(16).
[38] Paşca S P. Assembling human brain organoids[J]. Science, 2019,363(6423):126.
[39] Bagley J A, Reumann D, Bian S, et al. Fused cerebral organoids model interactions between brain regions[J]. Nature Methods, 2017,14(7):743-751.
[40] Birey F, Andersen J, Makinson C D, et al. Assembly of functionally integrated human forebrain spheroids[J]. Nature, 2017,545(7652):54-59.
[41] Miura Y, Li M, Birey F, et al. Generation of human striatal organoids and cortico-striatal assembloids from human pluripotent stem cells[J]. Nature Biotechnology, 2020,38(12):1421-1430.
[42] Andersen J, Revah O, Miura Y, et al. Generation of Functional Human 3D Cortico-Motor Assembloids[J]. Cell, 2020,183(7):1913-1929.
[43] Ronan J L, Wu W, Crabtree G R. From neural development to cognition: unexpected roles for chromatin[J]. Nature Reviews Genetics, 2013,14(5):347-359.
[44] Chesnutt C, Burrus L W, Brown A M C, et al. Coordinate regulation of neural tube patterning and proliferation by TGF β and WNT activity[J]. Developmental Biology, 2004,274(2):334-347.
[45] Brady M V, Vaccarino F M. Role of SHH in Patterning Human Pluripotent Cells towards Ventral Forebrain Fates[J]. Cells, 2021,10(4).
[46] Gurdon J B, Bourillot P Y. Morphogen gradient interpretation[J]. Nature, 2001,413(6858):797-803.
[47] Driever W, Nüsslein-Volhard C. A gradient of bicoid protein in Drosophila embryos[J]. Cell, 1988,54(1):83-93.
[48] CRICK F. Diffusion in Embryogenesis[J]. Nature, 1970,225(5231):420-422.
[49] Wolpert L, Lewis J H. Towards a theory of development[J]. Fed Proc, 1975,34(1):14-20.
[50] Rogers K W, Schier A F. Morphogen Gradients: From Generation to Interpretation[J]. Annual Review of Cell and Developmental Biology, 2011,27(1):377-407.
[51] Christian J L. Morphogen gradients in development: from form to function[J]. Wiley Interdiscip Rev Dev Biol, 2012,1(1):3-15.
[52] Menendez L, Yatskievych T A, Antin P B, et al. Wnt signaling and a Smad pathway blockade direct the differentiation of human pluripotent stem cells to multipotent neural crest cells[J]. Proc Natl Acad Sci U S A, 2011,108(48):19240-19245.
[53] Chambers S M, Mica Y, Lee G, et al. Dual-SMAD Inhibition/WNT Activation-Based Methods to Induce Neural Crest and Derivatives from Human Pluripotent Stem Cells[J]. Methods Mol Biol, 2016,1307:329-343.
[54] Libby A, Joy D A, Elder N H, et al. Axial Elongation of Caudalized Human Organoids Mimics Neural Tube Development[J]. bioRxiv, 2020:2020-2023.
[55] Girgin M U, Broguiere N, Mattolini L, et al. Gastruloids generated without exogenous Wnt activation develop anterior neural tissues[J]. Stem Cell Reports, 2021,16(5):1143-1155.
[56] Cederquist G Y, Asciolla J J, Tchieu J, et al. Specification of positional identity in forebrain organoids[J]. Nat Biotechnol, 2019,37(4):436-444.

[57] Bhatia S N, Ingber D E. Microfluidic organs-on-chips[J]. Nature Biotechnology, 2014,32(8):760-772.

[58] Yu F, Hunziker W, Choudhury D. Engineering Microfluidic Organoid-on-a-Chip Platforms: Micromachines[Z]. 2019: 10.

[59] Wu Q, Liu J, Wang X, et al. Organ-on-a-chip: recent breakthroughs and future prospects[J]. BioMedical Engineering OnLine, 2020,19(1):9.

[60] Saorin G, Caligiuri I, Rizzolio F. Microfluidic organoids-on-a-chip: The future of human models[J]. Seminars in Cell & Developmental Biology, 2023,144:41-54.

[61] Park J, Lee B K, Jeong G S, et al. Three-dimensional brain-on-a-chip with an interstitial level of flow and its application as an in vitro model of Alzheimer's disease[J]. Lab Chip, 2015,15(1):141-150.

[62] Zhu Y, Wang L, Yu H, et al. In situ generation of human brain organoids on a micropillar array[J]. Lab Chip, 2017,17(17):2941-2950.

[63] Wang Y, Wang L, Zhu Y, et al. Human brain organoid-on-a-chip to model prenatal nicotine exposure[J]. Lab Chip, 2018,18(6):851-860.

[64] Khan I, Prabhakar A, Delepine C, et al. A low-cost 3D printed microfluidic bioreactor and imaging chamber for live-organoid imaging[J]. Biomicrofluidics, 2021,15(2):24105.

[65] Cho A N, Jin Y, An Y, et al. Microfluidic device with brain extracellular matrix promotes structural and functional maturation of human brain organoids[J]. Nat Commun, 2021,12(1):4730.

[66] Karzbrun E, Kshirsagar A, Cohen S R, et al. Human Brain Organoids on a Chip Reveal the Physics of Folding[J]. Nat Phys, 2018,14(5):515-522.

[67] Ao Z, Cai H, Havert D J, et al. One-Stop Microfluidic Assembly of Human Brain Organoids To Model Prenatal Cannabis Exposure[J]. Anal Chem, 2020,92(6):4630-4638.

[68] Ao Z, Cai H, Wu Z, et al. Tubular human brain organoids to model microglia-mediated neuroinflammation[J]. Lab Chip, 2021,21(14):2751-2762.

[69] Cai H, Ao Z, Wu Z, et al. Intelligent acoustofluidics enabled mini-bioreactors for human brain organoids[J]. Lab Chip, 2021,21(11):2194-2205.

[70] Rifes P, Isaksson M, Rathore G S, et al. Modeling neural tube development by differentiation of human embryonic stem cells in a microfluidic WNT gradient[J]. Nat Biotechnol, 2020,38(11):1265-1273.

[71] Nishida A, Furukawa A, Koike C, et al. Otx2 homeobox gene controls retinal photoreceptor cell fate and pineal gland development[J]. Nature Neuroscience, 2003,6(12):1255-1263.

[72] Thakuri P S, Liu C, Luker G D, et al. Biomaterials-Based Approaches to Tumor Spheroid and Organoid Modeling[J]. Advanced Healthcare Materials, 2018,7(6):1700980.

[73] Oksdath M, Perrin S L, Bardy C, et al. Review: Synthetic scaffolds to control the biochemical, mechanical, and geometrical environment of stem cell-derived brain organoids[J]. APL Bioeng, 2018,2(4):41501.

[74] Layrolle P, Payoux P, Chavanas S. Message in a Scaffold: Natural Biomaterials for Three-Dimensional (3D) Bioprinting of Human Brain Organoids: Biomolecules[Z]. 2023: 13.

[75] Liu C, Xia Z, Czernuszka J T. Design and Development of Three-Dimensional Scaffolds for Tissue Engineering[J]. Chemical Engineering Research and Design, 2007,85(7):1051-1064.

[76] Lancaster M A, Corsini N S, Wolfinger S, et al. Guided self-organization and cortical plate

formation in human brain organoids[J]. Nat Biotechnol, 2017,35(7):659-666.

[77] Peña J, Corrales T, Izquierdo-Barba I, et al. Long term degradation of poly(ε-caprolactone) films in biologically related fluids[J]. Polymer Degradation and Stability, 2006,91(7):1424-1432.

[78] Lam C X, Teoh S H, Hutmacher D W. Comparison of the degradation of polycaprolactone and polycaprolactone–(β-tricalcium phosphate) scaffolds in alkaline medium[J]. Polymer International, 2007,56(6):718-728.

[79] Rothenbucher T, Gurbuz H, Pereira M P, et al. Next generation human brain models: engineered flat brain organoids featuring gyrification[J]. Biofabrication, 2021,13(1):11001.

[80] Xue J, Wu T, Dai Y, et al. Electrospinning and Electrospun Nanofibers: Methods, Materials, and Applications[J]. Chem Rev, 2019,119(8):5298-5415.

[81] Silva J C, Udangawa R N, Chen J, et al. Kartogenin-loaded coaxial PGS/PCL aligned nanofibers for cartilage tissue engineering[J]. Mater Sci Eng C Mater Biol Appl, 2020,107:110291.

[82] McIvor M J, O M F, Meenagh A, et al. 3D Fabrication and Characterisation of Electrically Receptive PCL-Graphene Scaffolds for Bioengineered In Vitro Tissue Models[J]. Materials (Basel), 2022,15(24).

[83] Mackenzie D. The History of Sutures[J]. Medical History, 1973,17(2):158-168.

[84] Frazza E J, Schmitt E E. A new absorbable suture[J]. J Biomed Mater Res, 1971,5(2):43-58.

[85] Qing C, Li Q, Xue N, et al. The Outlook of the Development of Innovative Products from Biocompatible Natural Spider Silk in the Beauty Thread-Lifting Industry[J]. Natural Products and Bioprospecting, 2021,11(1):21-30.

[86] Shabbirahmed A M, Sekar R, Gomez L A, et al. Recent Developments of Silk-Based Scaffolds for Tissue Engineering and Regenerative Medicine Applications: A Special Focus on the Advancement of 3D Printing: Biomimetics[Z]. 2023: 8.

[87] Madappura A P, Madduri S. A comprehensive review of silk-fibroin hydrogels for cell and drug delivery applications in tissue engineering and regenerative medicine[J]. Computational and Structural Biotechnology Journal, 2023,21:4868-4886.

[88] Lin M, Hu Y, An H, et al. Silk fibroin-based biomaterials for disc tissue engineering[J]. Biomater Sci, 2023,11(3):749-776.

[89] Martins J A, Lach A A, Morris H L, et al. Polydioxanone implants: A systematic review on safety and performance in patients[J]. J Biomater Appl, 2020,34(7):902-916.

[90] Vesvoranan O, Anup A, Hixon K R. Current Concepts and Methods in Tissue Interface Scaffold Fabrication[J]. Biomimetics (Basel), 2022,7(4).

[91] Moy R L, Waldman B, Hein D W. A review of sutures and suturing techniques[J]. J Dermatol Surg Oncol, 1992,18(9):785-795.

[92] Chambers S M, Fasano C A, Papapetrou E P, et al. Highly efficient neural conversion of human ES and iPS cells by dual inhibition of SMAD signaling[J]. Nature Biotechnology, 2009,27(3):275-280.

[93] Tomishima M. Neural induction - Dual SMAD inhibition[J]. 2008.

[94] Poon C. Measuring the density and viscosity of culture media for optimized computational fluid dynamics analysis of in vitro devices[J]. J Mech Behav Biomed Mater, 2022,126:105024.

[95] Jeon N L, Dertinger S K W, Chiu D T, et al. Generation of Solution and Surface Gradients

Using Microfluidic Systems[J]. Langmuir, 2000,16(22):8311-8316.

[96] Rifes P, Isaksson M, Rathore G S, et al. Modeling neural tube development by differentiation of human embryonic stem cells in a microfluidic WNT gradient[J]. Nature Biotechnology, 2020,38(11):1265-1273.

[97] Zeevaert K, Elsafi M M, Wagner W, et al. Cell Mechanics in Embryoid Bodies[J]. Cells, 2020,9(10).

[98] Liu M, Goldman G, MacDougall M, et al. BMP Signaling Pathway in Dentin Development and Diseases[J]. Cells, 2022,11(14).

[99] Smith J R, Vallier L, Lupo G, et al. Inhibition of Activin/Nodal signaling promotes specification of human embryonic stem cells into neuroectoderm[J]. Dev Biol, 2008,313(1):107-117.

[100] Rubenstein J R P. *Patterning and Cell Type Specification in the Developing CNS and PNS*[J]. Elsevier, 2013, 2013.

[101] Rosebrock D, Arora S, Mutukula N, et al. Enhanced cortical neural stem cell identity through short SMAD and WNT inhibition in human cerebral organoids facilitates emergence of outer radial glial cells[J]. Nat Cell Biol, 2022,24(6):981-995.

[102] Stoeckli E T. Morphogens and Neural Development[M]//BINDER M D, HIROKAWA N, WINDHORST U. Encyclopedia of Neuroscience. Berlin, Heidelberg: Springer Berlin Heidelberg, 2009:2397-2401.

[103] Miller M Q, McColl L F, Arul M R, et al. Assessment of Hedgehog Signaling Pathway Activation for Craniofacial Bone Regeneration in a Critical-Sized Rat Mandibular Defect[J]. JAMA Facial Plast Surg, 2019,21(2):110-117.

[104] Duval N, Vaslin C, Barata T C, et al. BMP4 patterns Smad activity and generates stereotyped cell fate organization in spinal organoids[J]. Development, 2019,146(14).

[105] Mak S K, Huang Y A, Iranmanesh S, et al. Small molecules greatly improve conversion of human-induced pluripotent stem cells to the neuronal lineage[J]. Stem Cells Int, 2012,2012:140427.

[106] Pellegrini L, Bonfio C, Chadwick J, et al. Human CNS barrier-forming organoids with cerebrospinal fluid production[J]. Science, 2020,369(6500).

[107] MacAulay N, Keep R F, Zeuthen T. Cerebrospinal fluid production by the choroid plexus: a century of barrier research revisited[J]. Fluids Barriers CNS, 2022,19(1):26.

[108] Dabbagh F, Schroten H, Schwerk C. In Vitro Models of the Blood-Cerebrospinal Fluid Barrier and Their Applications in the Development and Research of (Neuro)Pharmaceuticals[J]. Pharmaceutics, 2022,14(8).

[109] Hopwood N D, Pluck A, Gurdon J B. A Xenopus mRNA related to Drosophila twist is expressed in response to induction in the mesoderm and the neural crest[J]. Cell, 1989,59(5):893-903.

[110] Delmotte Q, Diabira D, Belaidouni Y, et al. Sonic Hedgehog Signaling Agonist (SAG) Triggers BDNF Secretion and Promotes the Maturation of GABAergic Networks in the Postnatal Rat Hippocampus[J]. Front Cell Neurosci, 2020,14:98.

[111] Borghese L, Dolezalova D, Opitz T, et al. Inhibition of notch signaling in human embryonic stem cell-derived neural stem cells delays G1/S phase transition and accelerates neuronal differentiation in vitro and in vivo[J]. Stem Cells, 2010,28(5):955-964.

[112] Fiorenzano A, Sozzi E, Birtele M, et al. Single-cell transcriptomics captures features of human midbrain development and dopamine neuron diversity in brain organoids[J]. Nat Commun, 2021,12(1):7302.

[113] Wen L, Tang F. Boosting the power of single-cell analysis[J]. Nature Biotechnology, 2018,36(5):408-409.

[114] Tao Y, Zhang S C. Neural Subtype Specification from Human Pluripotent Stem Cells[J]. Cell Stem Cell, 2016,19(5):573-586.

Supplementary materials

Name	Host	Isotype	Dilution	Source
SOX2	Rabbit	IgG	1:600	Abcam ab97959
MAP2	Chicken	IgY	1:600	Abcam ab5392
aPKCζ	Mouse	IgG2a	1:200	Santa Cruz sc-17781
OLIG2	Rabbit	IgG	1:500	Abcam ab136253
FOXG1	Rabbit	IgG	1:200	Abcam ab18259
FOXA2	Rabbit	IgG	1:30	Thermo PA5-35033

Table S1. Primary antibodies used for brain organoid immunostaining.

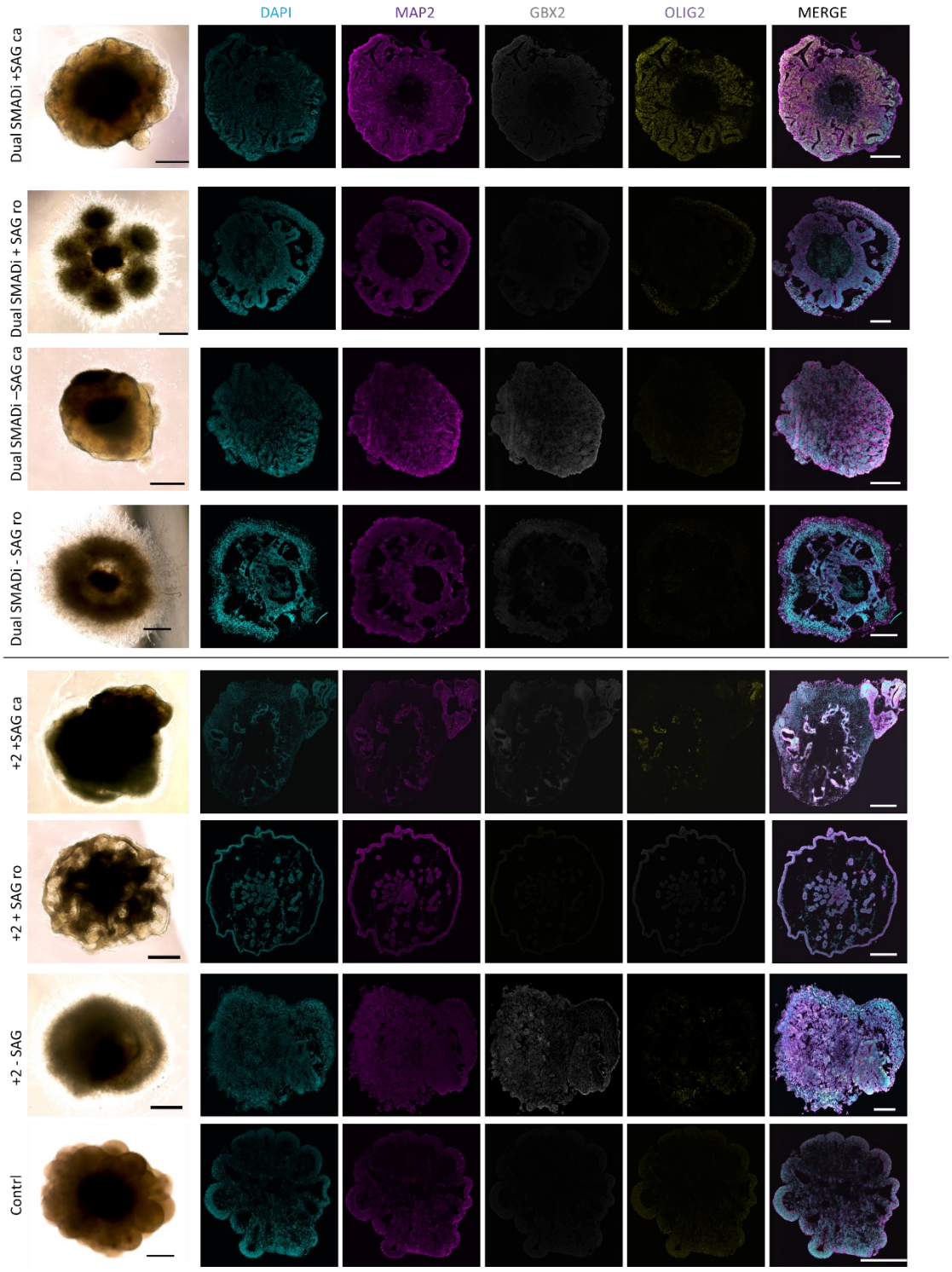


Figure S1. BF and confocal images of 20-day morphogens induced brain organoids following the plan of Figure 15. Scale bars = 500 µm.

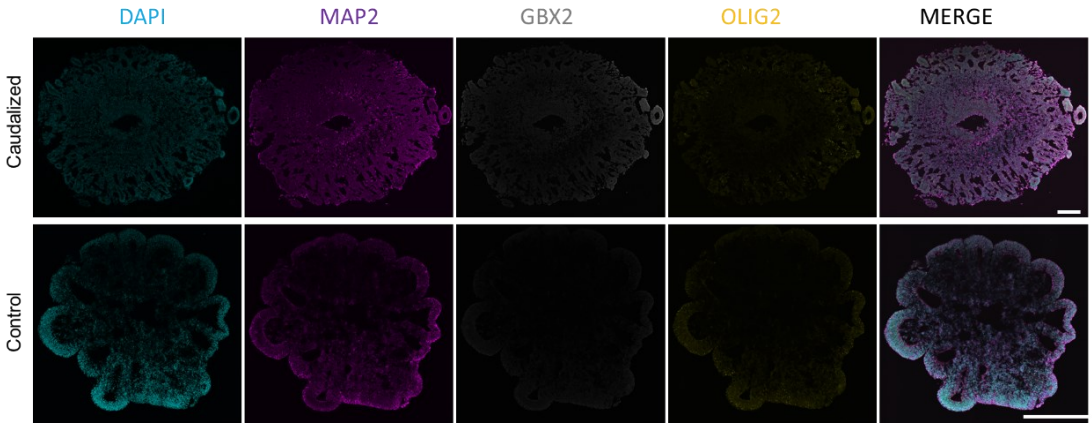


Figure S2. Confocal images of 20-day Pasca protocol caudalized organoid and control brain organoid stained by DAPI (cyan), MAP2 (magenta), GBX2 (grey) and OLIG2 (yellow). Scale bars = 500 μm.

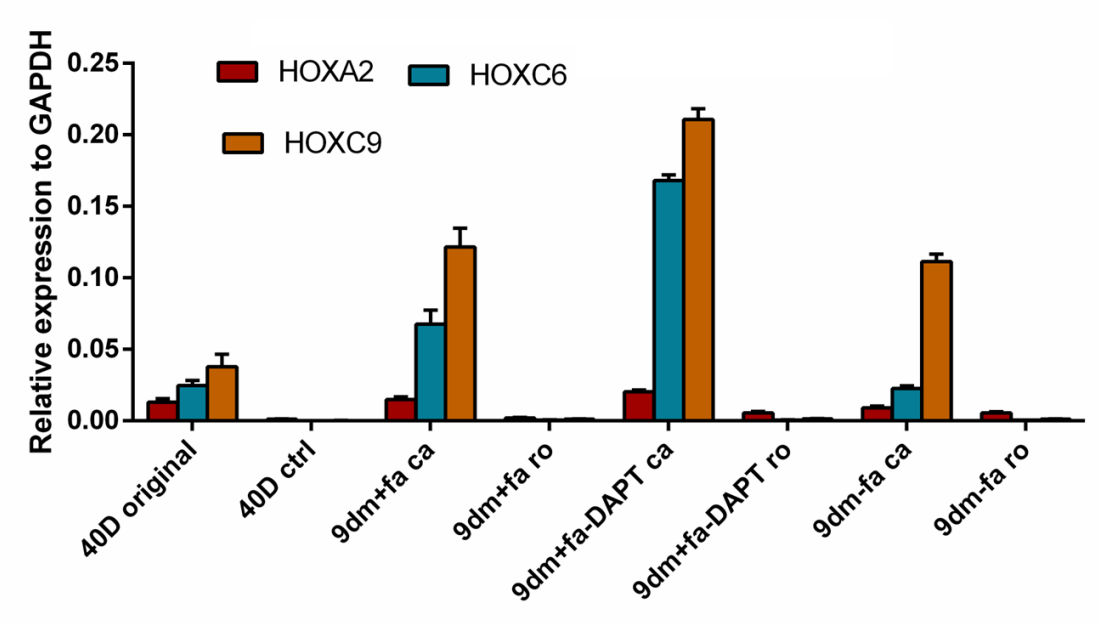


Figure S3. q-RT PCR result for 40-day brain organoids, N = 4.

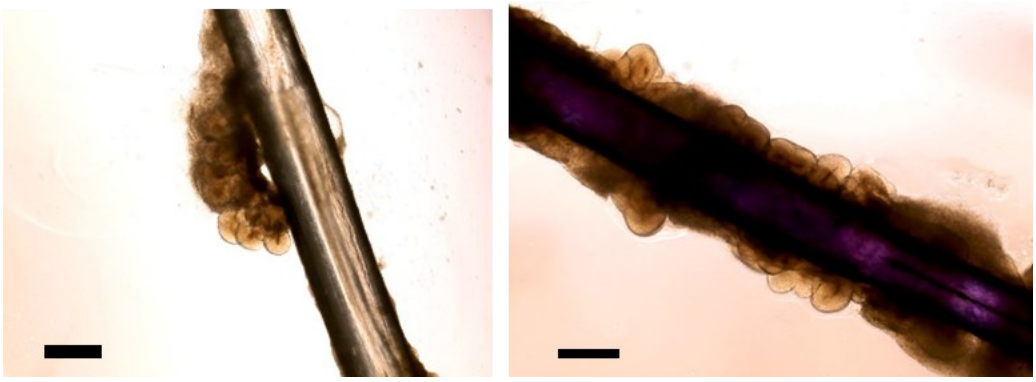


Figure S4. BF image of organoid peeled off the 20G PCL (left) but grew well on 20G PDO (right) scaffold. Scale bars = 500 μm.

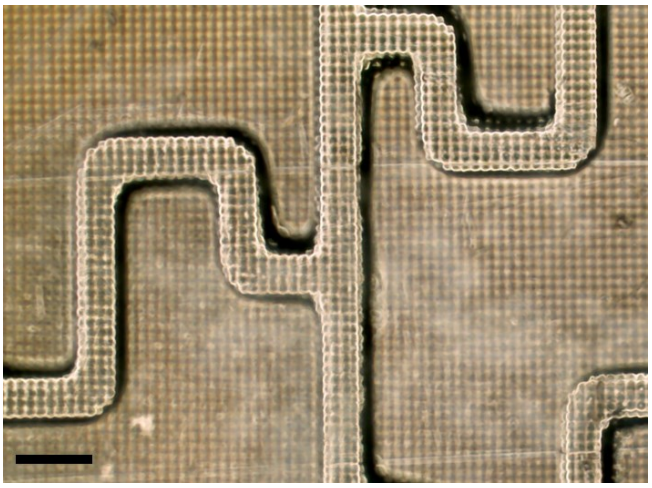


Figure S5. BF images of microfluidic PDMS chip surface. Scale bar = 500 μm.

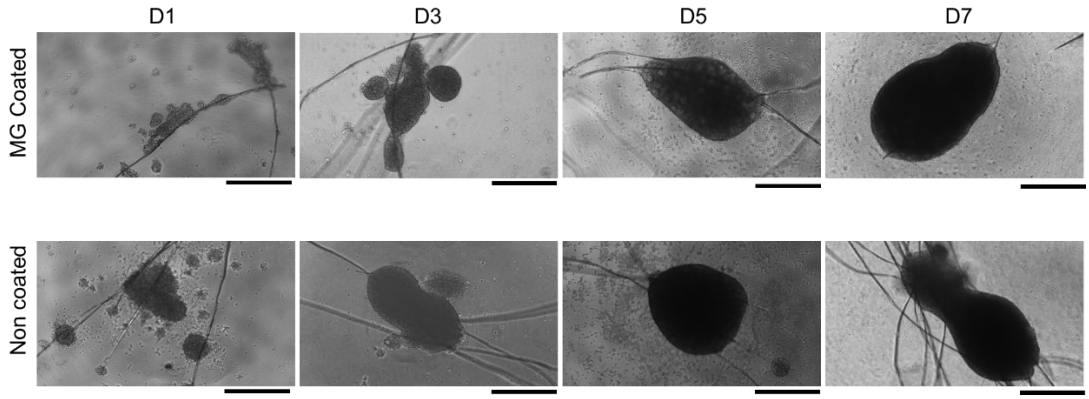


Figure S6. BF images of the MG coated and uncoated silk fibers regulating brain organoids growth. Scale bars = 500 μm.

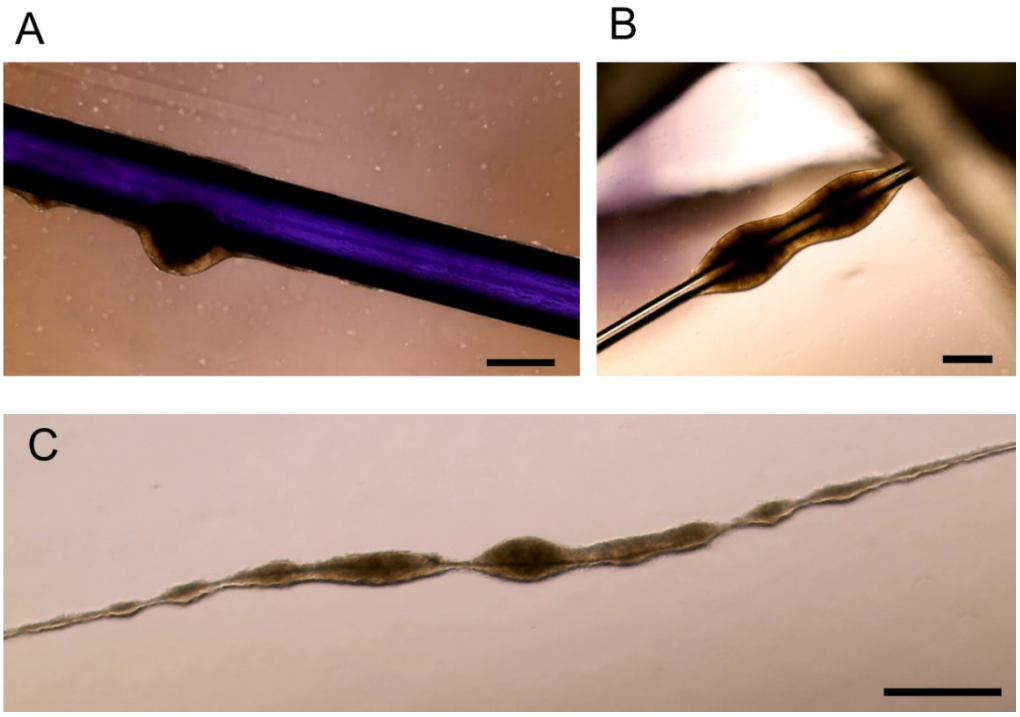


Figure S7. BF images of day 8 brain organoids growing on **A)** 20G PDO, **B)** 27G PDO, and **C)** silk fiber without appropriate seeding strategies. Scale bars = 500 μm.